Title
Valley-scale morphology drives differences in fluvial sediment budgets and incision rates during contrasting flow regimes

Authors
Weber, Matthew D
Pasternack, Gregory B

Publication Date
2017-03-01

DOI
10.1016/j.geomorph.2017.03.018

Peer reviewed

Valley-scale morphology drives differences in fluvial sediment budgets and incision rates during contrasting flow regimes

M. D. Weber and G. B. Pasternack*

University of California, Davis, One Shields Avenue, Davis, CA 95616, USA

* Corresponding author. Tel.: +1 (530) 302-5658
E-mail: gpast@ucdavis.edu

Cite as: Weber, M. D., Pasternack, G. B. in press. Valley-scale morphology drives differences in fluvial sediment budgets and incision rates during contrasting flow regimes. Geomorphology, http://dx.doi.org/10.1016/j.geomorph.2017.03.018

Abstract

High-resolution topographic surveys using LiDAR and multibeam sonar can be used to characterize and quantify fluvial change. This study used repeat surveys to explore how topographic change, fluvial processes, sediment budgets, and aggradation and incision rates vary across spatial scales and across two contrasting decadal flow regimes in a regulated gravel/cobble river. A novel method for quantifying digital elevation model uncertainty was developed and applied to a topographic change detection analysis from 2006/2008 to 2014. During this period, which had four modest ~3-5 year floods, most sediment was laterally redistributed through bank erosion and channel migration. Erosion primarily occurred in the floodplain (97,000 m^3), terraces (80,000 m^3), and lateral bars (58,000 m^3); while deposition occurred in the adjacent pools (73,000 m^3), fast glides (48,000 m^3), and runs (36,000 m^3). In contrast, significantly higher magnitude and longer duration floods from 1999 to 2006/2008 caused sediment to be displaced longitudinally, with the upstream reaches exporting sediment and the downstream reaches aggrading. The river maintained floodplain connectivity during both periods, despite different processes dominating the type of connectivity. Larger floods promoted overbank scour and avulsion, while smaller floods promoted bank erosion and lateral migration. This study explores and illustrates how the geomorphic response to contrasting flood regimes in a nonuniform river is highly dependent on which landforms are controlling hydraulics.

Keywords: topographic change detection; DEM differencing; river morphology; fluvial sediment budgets

1. Introduction

Gravel/cobble-bedded rivers with diverse fluvial landforms exist worldwide (Shen et al., 1981; Buffington and Montgomery, 1999; Wheaton et al., 2015) and have been highly degraded by cumulative anthropogenic impacts on all aspects of their ecogeomorphology (Ligon et al., 1995; Liébault and Piégay, 2001; Hancock, 2002; Lisle and Church, 2002). Nevertheless, these systems remain important because of their ecosystem functions and services, including aquatic habitat provision and renewal, riparian inundation, fish passage, sediment and nutrient outflux, local land loss, flood control, water supply, and navigation (e.g., Boulton et al., 2008; Arthington et al., 2010).

While much effort has been put into understanding the physics, geomorphology, and sediment transport of uniform gravel river channels (often using rectangular, uniform flumes; e.g., Parker, 1979; Wilcock, 1997; Millar, 2005), Ashworth and Ferguson (1986) observed a lack of studies that described and explained nonuniform rivers, including their morphodynamic patterns and mechanisms. That essential finding holds today, though meaningful progress has been made with flume experiments (e.g., Wu and Yeh, 2005; Wilkinson et al., 2008; Tal and Paola, 2010), numerical modeling (e.g., Nicholas et al., 2013; Oorschot et al., 2015), and field-based approaches (e.g., Carbonneau et al., 2012; Pasternack and Wyrick, 2016). More recently, Kleinhans (2010) reviewed studies of river patterns and concluded that the remaining inability to obtain dynamic meandering and braiding in laboratory experiments and physics-based models is indicative of our lack of understanding of morphodynamic mechanisms. Furthermore, White et al. (2010) compiled literature and evidence that make the case against assuming uniform flow for understanding many gravel rivers, and Gonzalez and

Pasternack (2015) showed that cross-sectional sampling as a ubiquitous methodology in fluvial geomorphology does not yield representative gravel-river attributes the way it is often assumed. Clearly, different approaches are needed to take the next steps to improve our understanding of nonuniform gravel/cobble rivers.

Thanks to technological advances (Passalacqua et al., 2015), submeter-scale topographic mapping of shallow gravel/cobble rivers has rapidly escalated with the emergence of commercially available multibeam sonar (MBS) systems (Hazel et al., 2010; Hensleigh, 2014), airborne bathymetric LiDAR (Hilldale and Raff, 2008; Mandlburger et al., 2015), terrestrial laser scanning (Vericat et al., 2014; Williams et al., 2014), structure-from-motion collected with unmanned aerial vehicles (Westoby et al., 2012; Fonstad et al., 2013; Javernick et al., 2014), and multispectral remote sensing data (Legleiter et al., 2009). These surveying methods allow researchers to explore the diversity and patterning of fluvial landforms (e.g., Wyrick and Pasternack, 2014; Casado et al., 2015; Brown and Pasternack, 2017), simulate how nonuniform topography drives a diversity of hydraulic patch behaviors (Strom et al., 2016), and more accessibly obtain repeat topographic surveys in support of topographic change detection (TCD) to reveal fluvial morphodynamics (e.g., Wheaton et al., 2013; Mandlburger et al., 2015; Wyrick and Pasternack, 2015).

Many gravel/cobble rivers behave differently than assumed because they have multiple layers of nested topographic heterogeneity (Gangodagamage et al., 2007; Brown and Pasternack, 2017). This means that the topographic patterns that steer flow within the base-flow channel are not the same as those for the larger bankfull channel or the floodprone valley– drawing on three common scales of scientific interest. This concept of stage-dependent topographic steering of flow produces patches of diverse hydraulic behaviors that change as flow increases and different landforms yield or take control of flow paths (Macwilliams et al., 2006; Strom et al., 2016). Brown and Pasternack (2014) applied this concept to explain topographic change and described bedload deposition mechanisms in a mountain river. This finding provides the impetus to explore fluvial morphodynamics at multiple sites, across a range of discharges, and using high-resolution topographic mapping to better understand the spatial structure of fluvial topographic change.

Considering this emerging understanding, we present and analyze novel field results comparing how fluvial morphodynamics in a topographically heterogeneous gravel-bed river corridor differ when forced by two significantly different hydrologic regimes. Both regimes involved a similar average annual runoff; but in the first period the water was distributed with larger floods and lower base flows, while the second period had long durations of moderate base flows and a few short, modest floods. This study illustrates how the geomorphic response to contrasting flood regimes in a nonuniform river is highly dependent on which landforms are activated and for how long.

1.1. Modern topographic change detection methods

In a topographic change detection (TCD) analysis (sometimes referred to as a geomorphic change detection analysis or GCD), two digital elevation models (DEMs) are differenced, and the raw results are adjusted based on an estimate of uncertainty within each DEM. Currently, most TCD analyses involve differencing raster-based

DEMs with spatially distributed error estimates. Researchers generally use one of the following strategies to account for DEM uncertainty: applying the fuzzy inference system (FIS) presented by Wheaton et al. (2010), using bootstrapping or Monte Carlo simulation to create multiple realizations of the DEM (Wechsler and Kroll, 2006; Wheaton et al., 2008), developing error functions based on the survey method and measures of topographic variability (Heritage et al., 2009; Milan et al., 2011; Carley et al., 2012), or using a geostatistical approach such as kriging (Kraus et al., 2006; Mandlburger et al., 2015). All the methods above represent legitimate ways to incorporate uncertainty into a TCD analysis.

No proposed method can unequivocally account for the uncertainty associated with a sampled topographic surface. Thus, each method has its limitations. The FIS relies on user-defined error thresholds and values to apply to combinations of categories (e.g., low/high point density or gentle/steep slopes) to prescribe a level of vertical elevation uncertainty. This provides a framework for incorporating multiple layers of uncertainty, but submeter resolution data sets may allow the development of deterministic statistical measures of uncertainty, which reduce the subjective nature of FIS. Bootstrapping methods are useful for interpreting the sensitivity of the resulting topographic map by subsampling the data, but bootstrapping methods are computationally expensive to create confidence intervals for large data sets. Field campaigns that relate spatial uncertainty to topographic variables are infeasible for large topographic surveys (e.g., >10 km of river corridor) and using past reported values may be insufficient given the unique characteristics of each landscape and survey method. Lastly, surfaces made using kriging do not adhere to the actual survey point data, which may not be appropriate for high-resolution data in steep and topographically complex terrain. With these concerns in mind, this study developed a new deterministic and efficient approach to characterize uncertainty using traditional statistical metrics at the raster-cell level.

1.2. Study objectives

The purpose of this study was to use the lower Yuba River (LYR), a regulated gravel-cobble river in northern California, as a testbed to explore gravel/cobble river morphodynamics during two decadal time periods with contrasting flow regimes. The specific scientific objectives were to compare topographic change at multiple spatial scales during each time period by (i) differentiating sediment budgets, (ii) calculating rates of vertical change for different inundated areas, and (iii) identifying the landforms that were the sources and sinks of sediment.

The two time periods analyzed were 1999 to 2006/2008 (time period 1) and 2006/2008 to 2014 (time period 2). Carley et al. (2012), Wyrick and Pasternack (2015), and Pasternack and Wyrick (2016) detailed the topographic change within LYR for time period 1, a period that included an ~23-year flood event (see section 2.4). This study analyzes topographic change in LYR using high-resolution topographic surveys (airborne NIR and bathymetric LiDAR and boat-based multibeam sonar) for time period 2, a period with four modest 3-5 year flood events (see section 2.4). Where applicable, we compared the results from time period 2 to the results for time period 1. Thus, the overall goal of this study was to revisit LYR, analyze topographic change during time period 2, and quantify fluvial topographic change and sediment budgets at multiple scales: the river segment (~100-1000 channel widths), geomorphic reach (~10-100 channel widths), and morphological unit (~0.1-10 channel widths) scales. We hypothesized that stage-dependent topographic steering would yield significantly different patterns of topographic change at each of the spatial scales for the two periods.

In the following sections, we provide an overview of LYR, topographic data collection efforts, and the analytical methods for this paper. More information on LYR, topographic data processing, and topographic change uncertainty methods are provided in the supplementary materials.

2. Study site – lower Yuba River

The Yuba River is a tributary of the Sacramento River in north-central California that drains 3480 km^2 of the western Sierra Nevada range (Fig. 1). The study segment is the alluvial lower Yuba River (LYR), a 37.1-km stretch that flows from east to west downstream of Englebright Dam to its confluence with the Feather River. This river segment is largely a single-threaded channel with ~20 emergent bars/islands at bankfull discharge, low sinuosity, high width-to-depth ratio, and slight to no entrenchment (Wyrick and Pasternack, 2012). Flows into LYR come primarily from three tributaries: the North, Middle, and South Yuba Rivers. Although the North Yuba tributary has a large reservoir that heavily regulates its outflow year-round, the absence of large reservoirs on the Middle and South Yuba tributaries translates to a broad range of discharges for LYR. Flows frequently (i.e., nearly annually) overtop Englebright Dam during large winter storms and spring snowmelt. Daguerre Point Dam (DPD), an 8-m-high run-of-the-river dam, is located near the middle of the study segment, 17.8 river

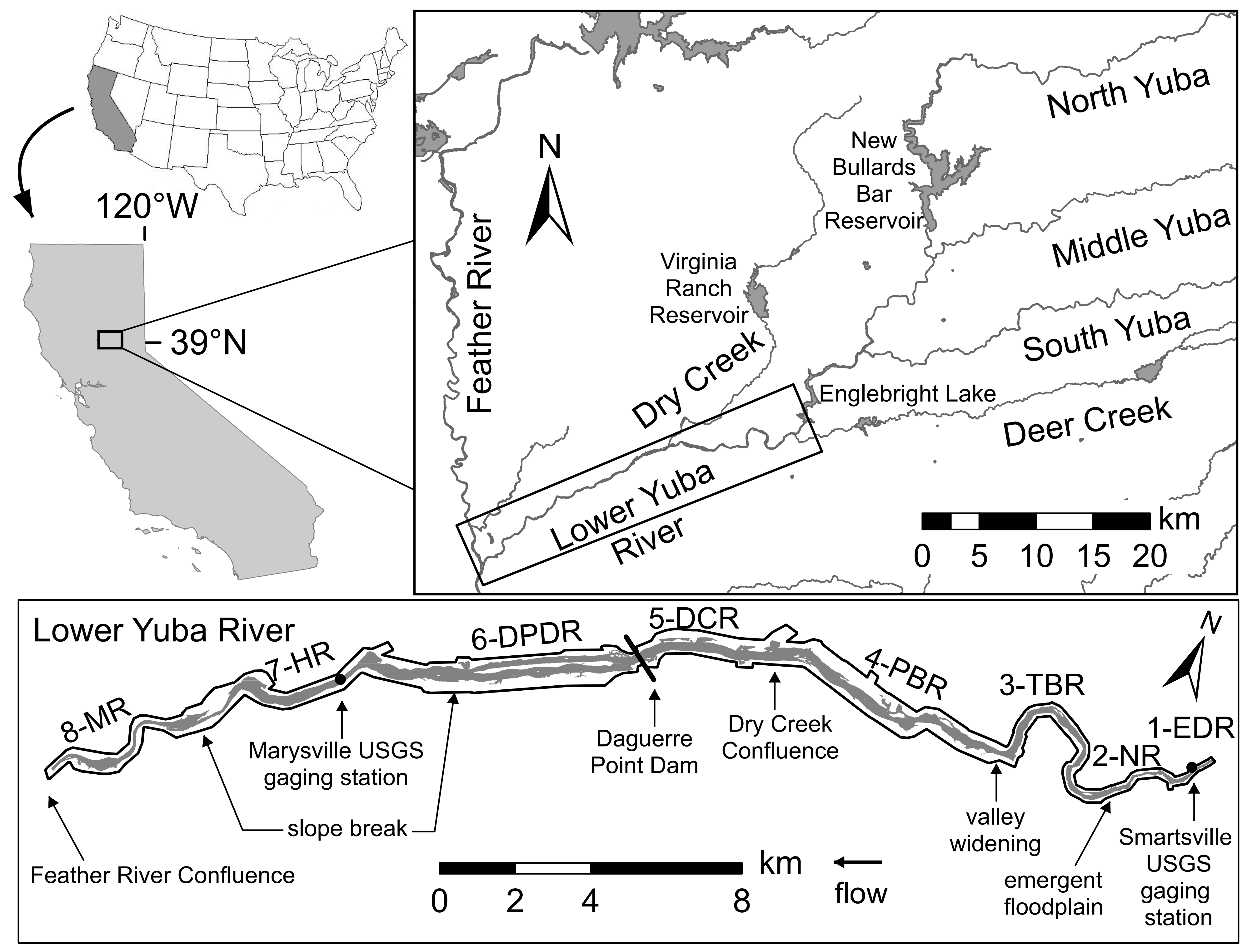
120°W
39°N
Feather River
N
Virginia Ranch Reservoir
New Bullards Bar Reservoir
North Yuba
Middle Yuba
South Yuba
Dry Creek
Englebright Lake
Deer Creek
Lower Yuba River
km
0 5 10 15 20
Lower Yuba River
8-MR
7-HR
6-DPDR
5-DCR
4-PBR
3-TBR
2-NR
1-EDR
N
Marysville USGS gaging station
Daguerre Point Dam
Dry Creek Confluence
valley widening
emergent floodplain
Smartsville USGS gaging station
slope break
Feather River Confluence
km
0 2 4 8
flow

kilometers (RKm) upstream from the Feather River. Storage behind DPD is filled with sediment, allowing bedload to pass downstream during flood events.

2.1. Geomorphic reaches

Wyrick and Pasternack (2012) identified eight geomorphic reaches within LYR based on the location of tributary junctions and changes in lateral confinement and bed slope. The Englebright Dam reach (1-EDR) and Narrows reach (2-NR) define the upper portion of LYR, where the river corridor is confined within a steep-walled bedrock canyon. Because of the lack of alluvium, these reaches are excluded from the TCD analysis. The Timbuctoo Bend reach (3-TBR) marks the emergence of the alluvial river valley, followed by significant valley widening in the Parks Bar reach (4-PBR). The Deer Creek reach (5-DCR) and Daguerre Point Dam reach (6-DPDR) have the widest floodplain. Finally, in the Hallwood reach (7-HR) and Marysville reach (8-MR), the bed slope significantly decreases; and the river corridor becomes laterally constrained by levees that protect the City of Marysville. Geomorphic reach breaks are presented in Figs. 1 and 2, and more information on the geomorphic reaches is provided in the supplementary materials.

2.2. Morphological units

Morphological units (MUs) are distinct landforms delineated at the scale of ~0.1-10 channel widths. In-channel bed MUs (e.g., pool, riffle, and chute) for LYR were delineated by Wyrick et al. (2014) using a two-dimensional (2D) hydrodynamic model of the 2006/2008 topography at a base-flow discharge. Other MUs within the active valley corridor (e.g., medial bar, floodplain, and terrace) were mapped by Wyrick and

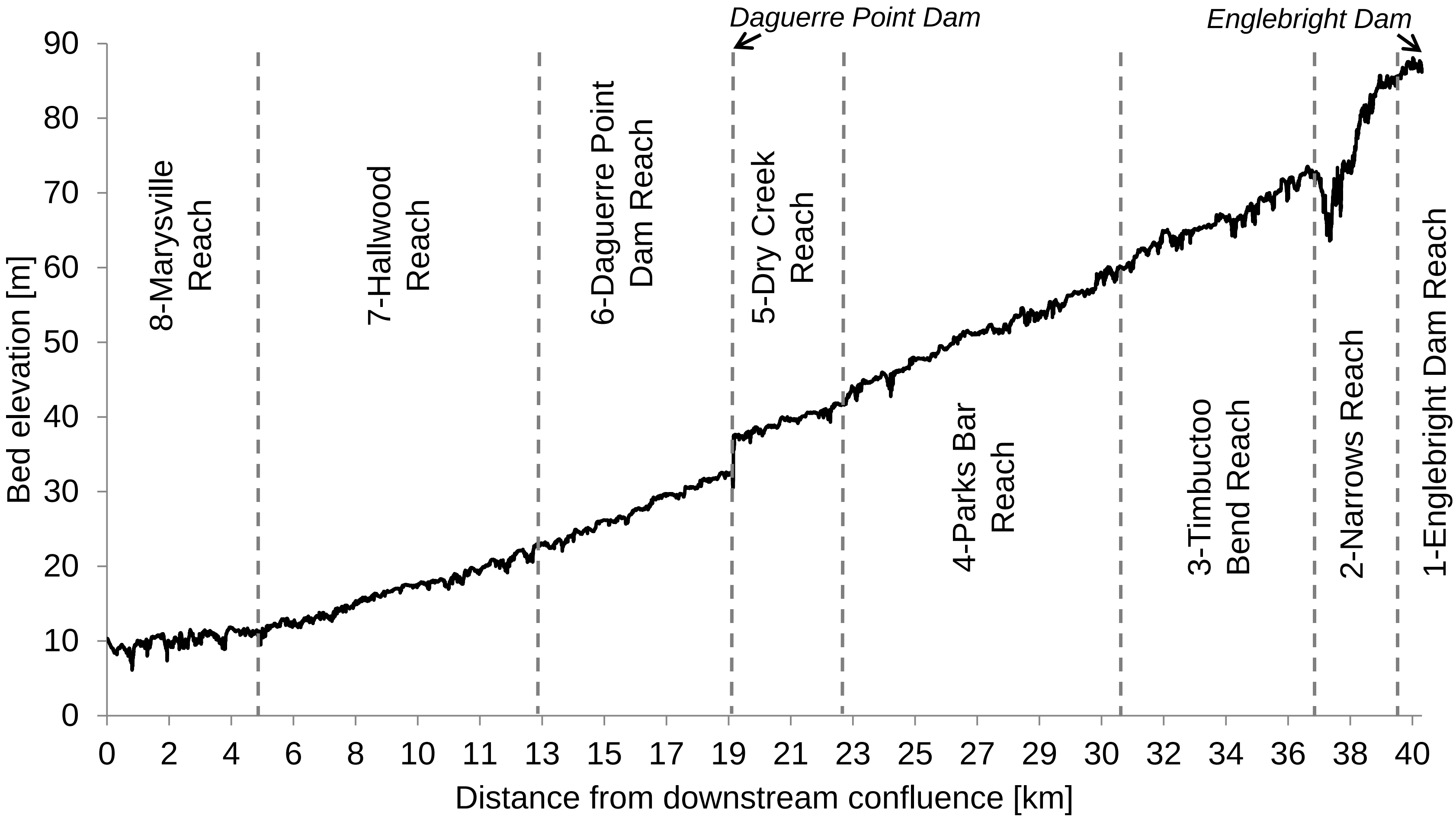

Daguerre Point Dam
Englebright Dam
Bed elevation [m]
Distance from downstream confluence [km]
8-Marysville Reach
7-Hallwood Reach
6-Daguerre Point Dam Reach
5-Dry Creek Reach
4-Parks Bar Reach
3-Timbuctoo Bend Reach
2-Narrows Reach
1-Englebright Dam Reach
0
10
20
30
40
50
60
70
80
90
0
2
4
6
8
10
11
13
15
17
19
21
23
25
27
29
30
32
34
36
38
40

Pasternack (2012) with the aid of 2D hydrodynamic modeling of flood discharges, which were reported by Barker (2012) and Abu-Aly et al. (2014). Thirty-one MUs were delineated and grouped into four categories defined by their inundation thresholds: in-channel bed MUs (inundated at a base-flow discharge), in-channel bank MUs (inundated at bankfull discharge), floodway MUs (inundated at the floodway filling discharge), and valley MUs (areas outside the floodway). A description of each of the MUs is provided in the supplementary materials.

2.3. Hydraulic mining and geomorphic history

The LYR has a complex geomorphic history because of the cumulative impacts of several historical human activities: deposition of large volumes of fill derived from historic hydraulic gold mining in the watershed (Gilbert, 1917; Adler, 1980; James, 2005; James et al., 2009), dredging of the ~4000-ha Yuba Goldfields and other areas in the ancestral river migration belt (James et al., 2009), installation of a high concrete arch sediment-barrier dam (Englebright Dam) in the canyon at the entrance to LYR in 1941 (Snyder et al., 2004, 2006), and moderate flow regulation from a suite of hydroelectric facilities throughout the catchment.

From 1852 to 1906, LYR aggraded by as much as 26 m near the exit of 3-TBR, declining to ~8 m of aggradation near the confluence with the Feather River (Adler, 1980). This large wedge of hydraulic mining sediment is up to 5 km in width through an area called the Yuba Goldfields. The California Debris Commission estimated that the LYR valley accumulated 10,380,000 m^3 of mining sediment, nearly 90% of which was still contained within the valley in 1980 (Adler, 1980). This period of rapid aggradation turned LYR into an anastomosing channel that was void of vegetation. Aggradation was followed by rapid channel incision after hydraulic mining ceased and the California Debris Commission began installing sediment control structures to limit sediment from being exported downstream and provide flood protection for the City of Marysville. Adler (1980) calculated that the channel from 1906-1912 underwent 33.5 cm/y of incision, which tapered off to an average of 6.4 cm/y from 1912 to 1979. Pasternack and Wyrick (2016) recently reported mean incision rates from 1999 to 2006/2008 with 3-TBR and 5-DCR incising ~4.5 and 5.9 cm/y, respectively. In the same study, the other geomorphic reaches analyzed were slightly aggrading, with 4-PBR, 6-DPDR, 7-HR, and 8-MR averaging ~0.1, 1.9, 1.6, and 0.1 cm/y of aggradation, respectively.

2.4. Flow regime

Hydrological records for LYR are available from three USGS flow gages: Smartsville (#11419000) below Englebright Dam, Marysville (#11421000) near the confluence with the Feather River, and Deer Creek (#11418500), a tributary. Pasternack et al. (2014) conducted a flood frequency analysis using data from 1970-2010. Relevant flows for this paper include 28.32 m^3/s as the representative base flow, 141.6 m^3/s as the estimated bankfull discharge, and 597.5 m^3/s as the floodplain-filling discharge. The return period of the bankfull discharge is ~1.25 years, which is more frequent than other similar rivers. The implication of this (and the high frequency of floodplain-filling flows) is that the channel may be undersized and flows spill onto the floodplain more often than expected.

Despite time period 1 (1999-2006/2008) and time period 2 (2006/2008-2014) having nearly similar total water and average annual flows (Table 1), the two time periods provide a contrast in the timing, duration, and magnitude of peak floods (Fig. 3). For the current study period (time period 2), four floodplain-filling events occurred, ranging from 838.2 to 1246 m^3/s instantaneous flow, which corresponds to ~3-5 year recurrence interval events (Wyrick and Pasternack, 2012) and 6-9 times bankfull discharge. These floods were short-duration events spread over three years. The prior TCD analysis (time period 1) included a maximum recorded instantaneous flow of 3207 m^3/s on 31 December 2005, which corresponds to a 23-year event and 22 times bankfull discharge. This event was preceded by a flood of 1480 m^3/s on 20 May 2005 and was followed by a series of three floods ranging from 637.0 to 1056 m^3/s in April 2006. Thus, time period 1 experienced three floods of much greater magnitude over a shorter period than time period 2. The duration above bankfull discharge was 200 days for time period 1 and 163 days for time period 2. The duration above floodplain-filling discharge was 18 days for time period 1 and 4 days for time period 2. Table 1 provides an overview of the peak annual flows for each time period, the average annual volume of water, and a characterization of each water year with respect to historical averages.

3. Methods

This study analyzed and compared topographic data from two high-resolution topographic surveys, one conducted in 2006/2008 and one conducted in 2014. To address the study objectives, we developed a new spatially distributed method for estimating topographic uncertainty for raster DEMs. This uncertainty analysis was applied to the two topographic data sets and the DEM difference raster computed from

Table 1

Summary of water year[a] statistics for the study period (time period 2 is shaded)

Water year[a]	Instantaneous peak (m^3/s)	Daily avg. peak (m^3/s)	Avg. volume (10^6 m^3/y)	Water year type
2000	642.0	608.8	1779.0	Above Average
2001	63.5	55.8	696.0	Dry
2002	149.3	142.7	1241.0	Below Average
2003	236.2	231.1	1830.0	Above Average
2004	418.9	345.5	1354.0	Below Average
2005	1480.0	1229.0	1829.0	Above Average
2006	3207.0	2384.0	4794.0	Wet
2007	375.0	283.2	904.0	Dry
2008	138.2	130.3	817.0	Dry
2009	566.3	356.8	1243.0	Below Average
2010	189.6	181.2	1422.0	Below Average
2011	875.0	761.7	3837.0	Wet
2012	961.1	603.1	1367.0	Below Average
2013	1246.0	628.6	1265.0	Below Average
2014	217.8	178.1	595.0	Dry
Period 1 ('00-'08)	3207.0	2384.0	1694.0	N/A
Period 2 ('09-'14)	1246.0	761.7	1621.0	N/A

[a]The California water year begins on 1 October and ends on 30 September. For example, water year 2000 began on 1 October 1999 and ended on 30 September 2000.

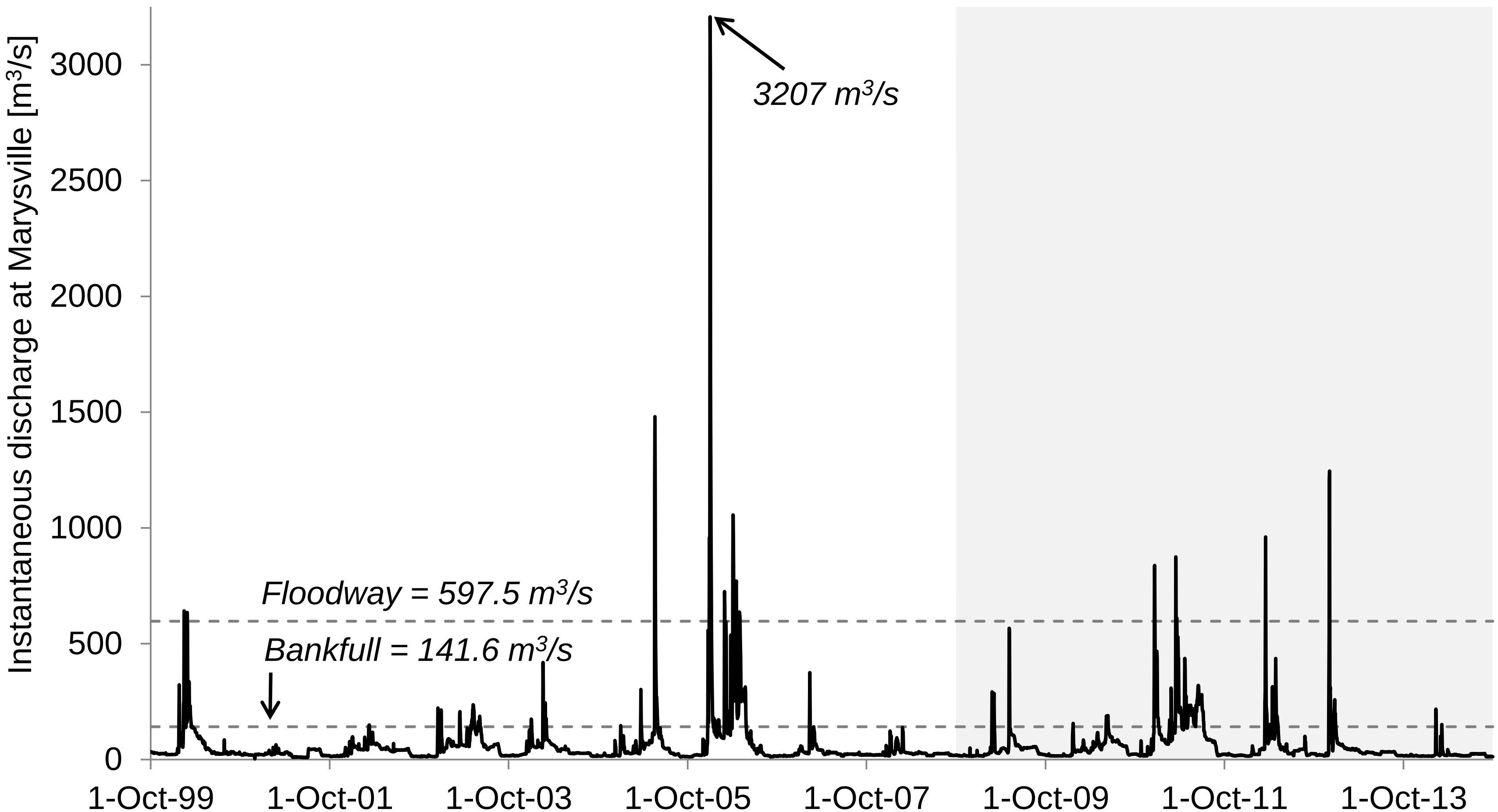

Instantaneous discharge at Marysville [m3/s]
3207 m3/s
Floodway = 597.5 m3/s
Bankfull = 141.6 m3/s
0
500
1000
1500
2000
2500
3000
1-Oct-99
1-Oct-01
1-Oct-03
1-Oct-05
1-Oct-07
1-Oct-09
1-Oct-11
1-Oct-13

them. Volumetric sediment budgets were calculated at multiple spatial scales to assess the patterns of erosion and deposition within LYR. The sediment budget for LYR assumes no sediment input from the upper watershed, as Englebright Dam blocks all bedload and Deer and Dry Creeks contribute negligible amounts of sediment. In addition, no landslides or other significant lateral sediment fluxes occurred from outside the TCD region. Thus, the sediment budget must result in net erosion with the value yielding the net volumetric export of sediment out of LYR to the Feather River.

At each of three relevant spatial scales, the river segment (~100-1000 channel widths), the geomorphic reach (~10-100 channel widths), and the morphological unit (~0.1-10 channel widths) scales, a series of analyses were conducted to assess the river's topographic adjustment. At the segment scale, longitudinal profiles of volumetric change and percent area of change aimed to provide an understanding of how patterns of erosion and deposition are organized. At the segment and geomorphic reach scales, the 2008 bankfull channel was delineated and used to stratify results into in-channel vs. overbank areas. This analysis aimed to provide insight into sediment connectivity between the channel and the floodplain and to help answer whether morphological diversity is maintained through channel migration or avulsion events. Furthermore, vertical topographic change rates were calculated across incrementally wetted areas provided by a 2D hydrodynamic model. These results were designed to explicitly test whether the river is becoming more entrenched by comparing the rate of vertical change at different inundation levels. Finally, at the morphological unit scale, volumetric sediment budgets were calculated to reveal the landforms that are the sources and sinks of sediment within LYR.

Notably, a different set of survey methods, point densities, and error analyses were used for time period 1 (Carley et al., 2012). Uncertainties for time period 1 are higher, as the first survey in 1999 did not involve meter-scale topographic mapping with terrestrial LiDAR. Nevertheless, the values reported are the best estimates of topographic change within LYR for each time period.

3.1. Topographic data collection

3.1.1. *2006/2008 surveys*

For the 2006/2008 DEM, 3-TBR was surveyed in 2006 using a robotic total station for terrestrial areas and wadable bathymetry, and boat-mounted single-beam sonar (SBS) was used for unwadable bathymetry. The reaches downstream of 3-TBR were primarily surveyed in 2008. Aero-Metric, Inc. (Seattle, WA) flew airborne near-infrared (NIR) LiDAR for terrestrial mapping on 21 September 2008 when flows were 24.4 m^3/s above DPD and 17.6 m^3/s below DPD (the difference caused by irrigation diversions at DPD). River bathymetry was primarily mapped by SBS, except for inaccessible areas that were surveyed by a real-time kinematic global positioning system (RTK-GPS) or robotic total station. The 2006/2008 surveying effort was reported by Carley et al. (2012) and is summarized in the supplementary materials.

3.1.2. *2014 Surveys*

The 2014 DEM involved a new survey of LYR during an extended drought that left LYR at its lowest point since new environmental flow schedules were fully implemented by the Lower Yuba River Accord in 2008. Quantum Spatial, Inc. (Sheboygan, WI) collected airborne bathymetric LiDAR data (using combined NIR and green laser scanners) on 27

September 2014 when flows were 15.3 m^3/s above DPD and 11.3 m^3/s below DPD. Low flows allowed more of the river valley to be mapped by the NIR laser and reduced the depths required for the green laser to penetrate through the water column. To map the riverbed at depths greater than the green laser could penetrate, Seafloor Systems, Inc. (El Dorado Hills, CA) collected MBS data on 11-14 August 2014, when flows were 40.0 m^3/s above DPD and 22.7-24.5 m^3/s below DPD. The higher water levels facilitated overlapping of MBS and LiDAR data. Several days were spent using SBS and RTK-GPS survey points to map data gaps and areas where submerged vegetation precluded accurate aerial and sonar mapping. A full account of 2014 mapping efforts and post-processing of data is included in the supplementary materials. Data resolutions by land cover type are presented in Table 2 for the 2006/2008 DEM and the 2014 DEM.

3.2. DEM uncertainty for the 2006/2008-2014 TCD

Even though topographic data involves points, a raster cell is commonly the fundamental unit for most topographic change analyses. Topographic change is reported when elevation change within a raster cell, ΔZr, exceeds the level of detection (*LOD*) determined by the DEM uncertainty method.

The DEM uncertainty method developed for this study creates confidence limits for each raster cell using a traditional statistical approach for Gaussian distributions by calculating the standard error of the mean (*SEM*), yet this has not been done before in the published literature. The approach uses the density of the survey data, *N* (which is the number of surveyed ground points contained by each raster cell) and the standard deviation, *SD* (which is an estimate of the variability of the survey data, to calculate the

Table 2

Data resolution (pts/m^2) comparisons by land-cover type

Land cover	2006/2008 DEM	2014 DEM
Bare Earth	5.71	13.17
Water	0.59	5.12
Vegetated Ground	1.37	3.05

SEM; Eq. 1). The *SEM* is governed by a simple equation that is functionally equivalent to doing statistical bootstrapping, where a sample mean is calculated from a specified number of observations (*N*) that are pulled randomly from a population of data with a given standard deviation (*SD*). If this is done enough times, the resulting distribution of errors in sample mean is characterized by the *SEM*, which follows a normal distribution. An *SEM* is calculated for each survey period (Eq. 1) for every raster cell, and then the two *SEM* rasters are combined at the 95% confidence interval to obtain the *LOD* (Eq. 2),

$$SEM_{2014} = \frac{SD_{2014}}{\sqrt{N_{2014}}} \tag{1}$$

$$LOD_{95} = \sqrt{(1.96 * SEM_{2008})^2 + (1.96 * SEM_{2014})^2} \tag{2}$$

where the subscripts on the right side of the equation are the survey year (Lane et al., 2003), and *SD* is an estimate of the variability of the data.

To apply Eqs. (1) and (2), *SD* is needed for each raster cell. This variability can come from at least two sources: topographic variability (e.g., substrate size or slope) or survey error (*SE*). For remote sensing methods like LiDAR and MBS, a significant proportion of the *SE* involves distinguishing between ground vs. nonground returns, which depends on the land cover. For this method, *SD* is determined by incorporating both sources of variability. Topographic variability, *SD_Z*, is calculated from the ground-classified point cloud for the area contained by each raster cell as well as by the method outlined in

Carley et al. (2012). The larger of the two *SD_Z* values is used. The *SE*s were calculated for different land cover classes (bare ground, water, and vegetated ground) and represent the ability for a survey method to correctly identify ground within each land cover. A detailed explanation of how the *SE*s were calculated is included in the supplementary materials. Lastly, both sources of variability are combined by taking the square root of the sum of the squares (Eq. 3):

$$SD_{2014} = \sqrt{(SD\_Z_{2014})^2 + (SE_{2014})^2} \quad (3)$$

An overview of the steps involved for the DEM uncertainty method is included below, and a visualization of the outputs is provided in Fig. 4.

1. Use a LiDAR or point cloud software package (e.g., LAStools or TerraScan) to classify all survey points as ground, vegetation, structure, or noise.
2. Use the ground classified points to create a raster DEM where *Zr* is the height in each raster cell (Fig. 4B).
3. Create a land-cover raster (Fig. 4C) from the point classifications, and assign the survey error (*SE*) associated with each land-cover class.
4. Calculate the topographic variability, *SD_Z*, in each raster cell using the approach by Milan et al. (2011) or Brasington et al. (2012) (Fig. 4E).
5. Calculate an estimate of the total variability, *SD*, by applying Eq. (3).
6. Create a raster with the number of ground points per raster cell, *N* (Fig. 4D).
7. Calculate the standard error of the mean, *SEM*, using Eq. (1) (Fig. 4F).

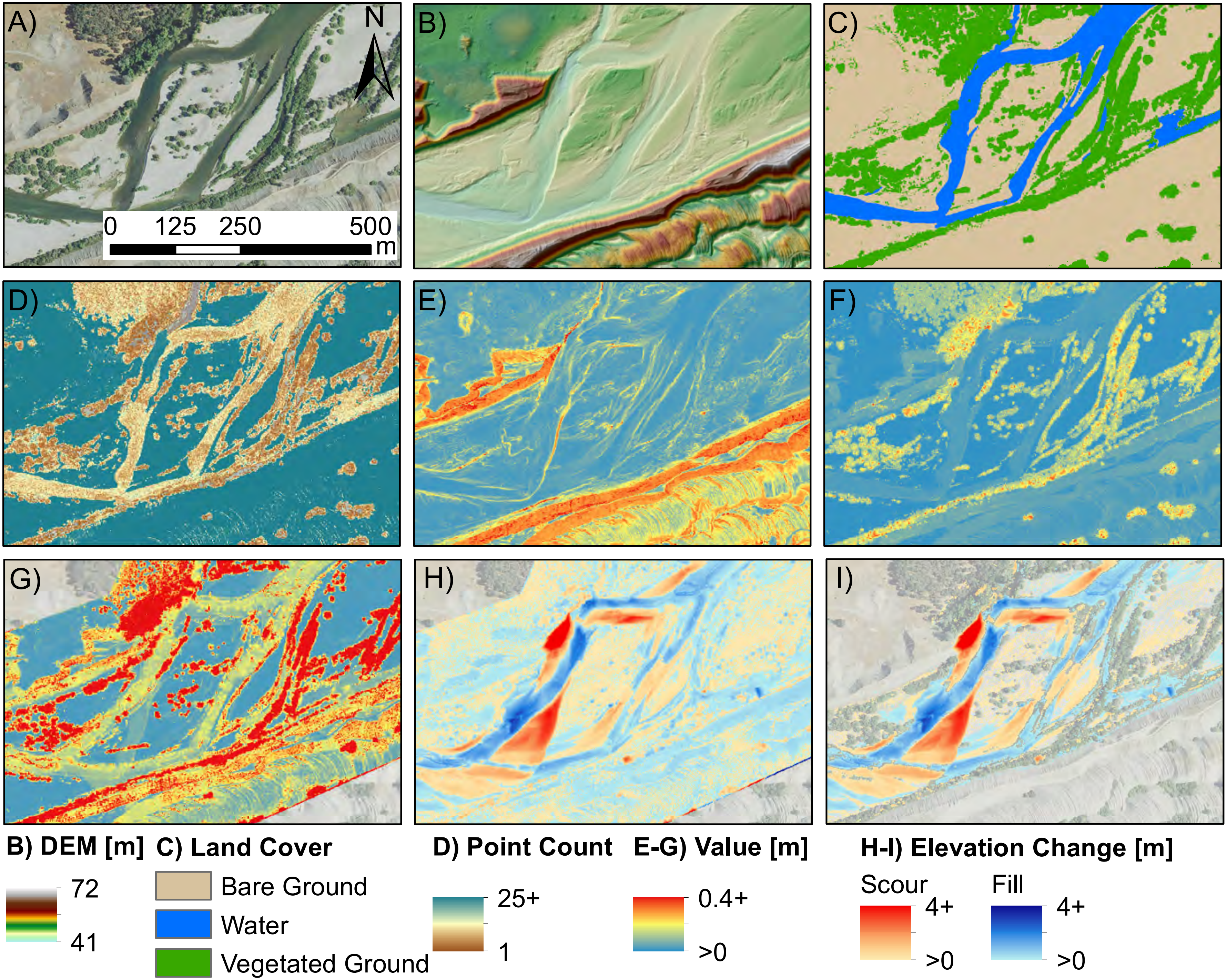
A)
N
0 125 250 500
m
B)
C)
D)
E)
F)
G)
H)
I)
B) DEM [m]
72
41
C) Land Cover
Bare Ground
Water
Vegetated Ground
D) Point Count
25+
1
E-G) Value [m]
0.4+
>0
H-I) Elevation Change [m]
Scour
4+
>0
Fill
4+
>0

8. Complete the steps above for each year's DEM. Then calculate the 95% confidence level of detection, LOD_{95}, using Eq. (2) (Fig. 4G).
9. Difference the two DEMs (Fig. 4H) and subtract the LOD_{95} raster values from the raw results to yield the statistically significant erosion or deposition that occurred within each raster cell (Fig. 4I).

3.3. *Sediment Budgeting*

After completing the DEM uncertainty analysis and subtracting the LOD_{95} from the raw DEM-difference raster, sediment budgets were created at river-segment, geomorphic-reach, and morphological-unit scales. This computation assumed no nontransport mechanisms of volumetric change, previously termed bed *deflation* or *contraction* and *inflation* or *dilation* (Merz et al., 2006; Marquis and Roy, 2012). In addition, if a raster cell erodes and then fills in between surveys, no change will be detected in that cell: a process known as compensating scour and fill (Lindsay and Ashmore, 2002).

3.3.1. *River-Segment Scale*

Longitudinal profiles of erosion and deposition were created by delineating the valley centerline in ArcGIS and creating regularly spaced rectangular station boxes (shown in the supplementary materials). The station boxes are orthogonal to the valley centerline, span the width of the river valley, and are 1.524 m in width. Their position along the valley centerline represents the distance upstream from the confluence with the Feather River. The total volume [m^3] of erosion and deposition within each station box was calculated, as well as the percent area of erosion, deposition, or no detectable level of change within the floodway. To explore the correlation between locations of peak erosion and deposition, the Pearson's product-moment correlation was calculated using the longitudinal series of erosion and deposition volumes. The correlation values range from -1 to 1, with positive values indicating that the locations of peak erosion and deposition coincide. A negative value indicates that peak locations of erosion coincide with the low values of deposition and vice versa. Lastly, the volumetric rate of change [m^3/y] for the entire study area was calculated for erosion and deposition. The difference between these two values represents the average rate of sediment eroded out of the LYR valley.

3.3.2. *Geomorphic-Reach Scale*

At the geomorphic-reach scale, the volumetric rate of change [m^3/y] was calculated for each geomorphic reach to understand the relative balance of erosion and deposition within each reach. Because 3-TBR was mapped in 2006, it is averaged over 8 years (2006-2014), while the rest of LYR is averaged over 6 years (2008-2014). Results were also stratified across in-channel vs. overbank areas. The in-channel areas are defined by a wetted area polygon determined by a 2D hydrodynamic model of the 2006/2008 topography at bankfull discharge (141.6 m^3/s). Lastly, net rates of vertical change were estimated by calculating the net volumetric rate of change [m^3/y] within a wetted area polygon developed by the 2D hydrodynamic model at several discharges (28.32, 141.6, 283.2, and 597.5 m^3/s; see below) and dividing by the inundated area [m^2] of the model to yield the average vertical change per year [mm/y]. This analysis was applied to the areas that are incrementally wetted as discharge increased from 28.32 m^3/s (base flow), 141.6 m^3/s (bankfull), 283.2 m^3/s (intermediate), and 597.5 m^3/s (floodplain filling) (Fig. 5B). For example, the values reported for the bankfull wetted area exclude the areas

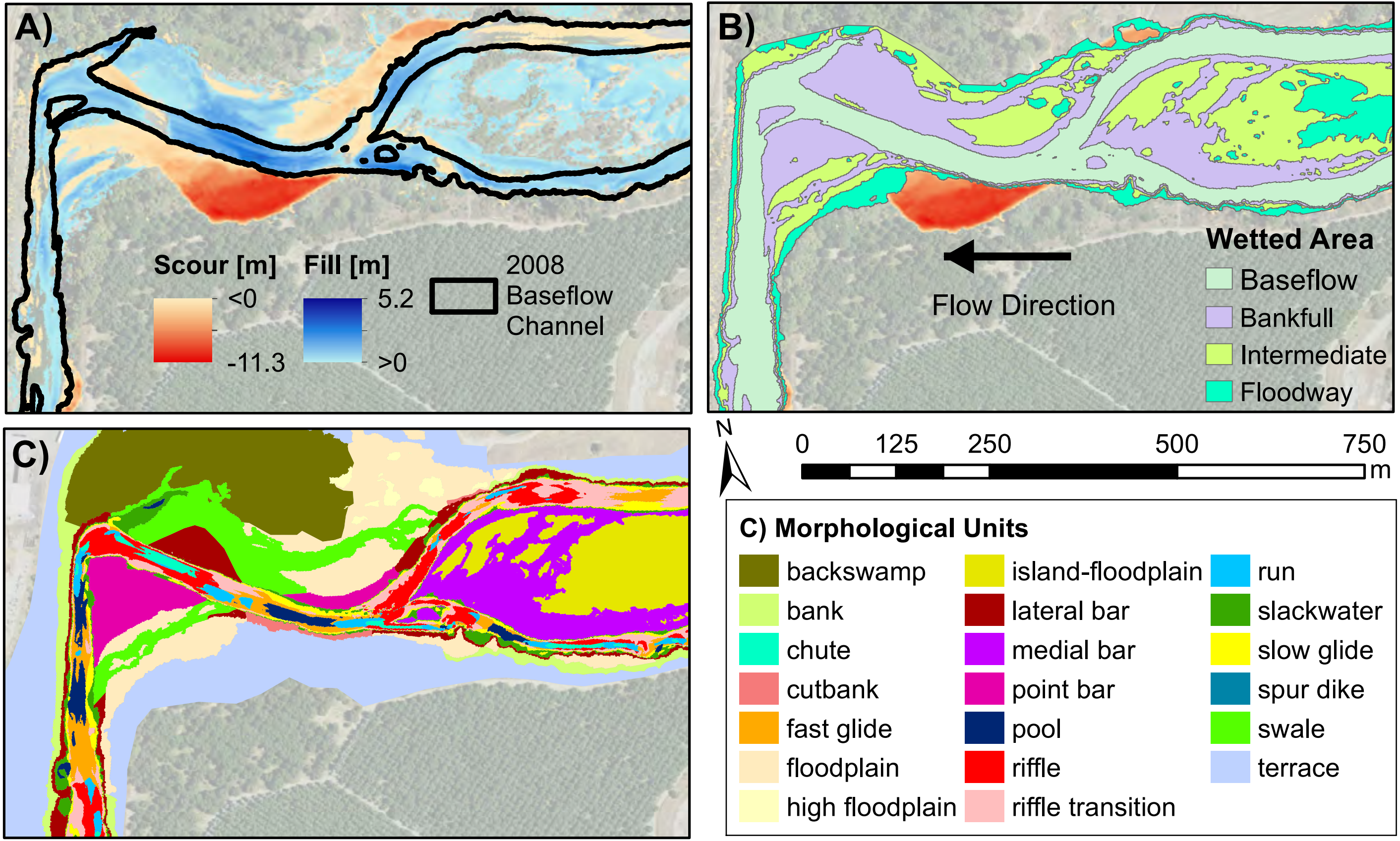
A)
Scour [m]
<0
-11.3
Fill [m]
5.2
>0
2008 Baseflow Channel
B)
Flow Direction
Wetted Area
Baseflow
Bankfull
Intermediate
Floodway
C)
N
0
125
250
500
750
m
C) Morphological Units
backswamp
bank
chute
cutbank
fast glide
floodplain
high floodplain
island-floodplain
lateral bar
medial bar
point bar
pool
riffle
riffle transition
run
slackwater
slow glide
spur dike
swale
terrace

that are wetted at base flow discharge. This analysis explores how vertical topographic change occurs at different positions within the river valley (e.g., how is the channel responding in contrast to different floodplain areas?) and provides estimates of valley-wide incision rates, which were previously reported by Adler (1980) and Pasternack and Wyrick (2016) discussed in section 2.3.

3.3.3. *Morphological-unit scale*

Sediment budgets presented at the morphological-unit scale were developed using the MUs discussed in section 2.2 and are expanded upon in the supplementary materials. The sediment budgets calculated for the MUs provide a summary of the topographic change that occurred to the former 2006/2008 landforms within LYR. This provides an understanding of the sources and sinks of sediment movement; however, it does not represent the net gain or loss of a morphological unit. For example, as a river channel migrates or avulses, new in-channel MUs are created in areas that were previously floodplain. Therefore, even though 2006/2008 pools may show net fill, this does not necessarily indicate that pool habitats have filled in or decreased overall. Instead, the former location of a pool filled, whereas a new pool may be created in an area that was previously floodplain. Further analysis would be needed to delineate the new 2014 MUs to assess net impacts to the MUs and is beyond the scope of this study.

4. Results

4.1. DEM Uncertainty

The *SE*s calculated by land cover type for the 2006/2008 to 2014 TCD were 0.039 m for bare ground and 0.074 m for water. A value of 0.30 m was chosen for vegetated ground, which comes from a review of the relevant literature for vertical error estimates for LiDAR in leaf-on forested settings (Reutebuch et al., 2003; Hodgson and Bresnahan, 2004; Gould et al., 2013; Tinkham et al., 2013; Edson and Wing, 2015). Figure 4 shows how uncertainty was influenced by land cover, point density, and topographic variability. In bare ground areas, point densities were high and survey errors were low, resulting in small raster elevation uncertainties, even in topographically complex areas. In vegetated areas, point densities were low and survey errors were high, yielding larger uncertainties.

4.2. River-Segment Scale

For the flow regime in time period 2, erosion was the dominant process in LYR. The TCD analysis estimates 103,000 m^3/y of erosion and 80,800 m^3/y of deposition within the LYR valley (i.e., in-channel and overbank areas), a net change of 22,200 m^3/y of erosion. This net change represents the average annual volume of sediment exported to the Feather River.

A comparison of net topographic change between in-channel vs. overbank areas revealed that, during time period 2, LYR was strongly depositional within the 2006/2008 bankfull channel, with a net topographic change of 20,300 m^3/y of deposition, and strongly erosional in the overbank region, with a net topographic change of 41,600 m^3/y of erosion. The large bank collapse in 7-HR accounts for 13,700 m^3/y of erosion, which is 13.3% of the total erosion within the LYR valley and 33.9% of the net erosion in the overbank areas.

The longitudinal series of deposition and erosion volumes for time period 2 show that the locations of peak values of deposition and erosion are moderately correlated with one another (Fig. 6). The Pearson's product-moment correlation of erosion and deposition volumes was 0.47 (p < 0.001). The longitudinal series of deposition and erosion by area (Fig. 7) shows significant variation, with erosion being the dominant process by area within 6-DPDR, deposition being the dominant process by area in 7-HR, and more balance across the other geomorphic reaches. Averaged across the entire floodway, 22% of the area experienced erosion, 25% experienced deposition, and 53% indicated no change.

4.3. Geomorphic-Reach Scale

At the geomorphic-reach scale, all reaches were net erosional for time period 2, except for 7-HR, which had a nearly equal balance of valley-wide erosion and deposition (Fig. 8B). The 5-DCR and 6-DPDR were the most imbalanced reaches with 51% and 77% more erosion than deposition, respectively. Every geomorphic reach during time period 2 was strongly erosional for overbank areas, but the results for in-channel areas vary by reach (Table 3). All in-channel areas of reaches were net depositional, except for 3-TBR (230 m^3/y of net erosion) and 6-DPDR (500 m^3/y of net erosion).

Rates of vertical change varied significantly by geomorphic reach and by the incremental wetted areas. The 2008 base-flow channel (wetted by 28.32 m^3/s) aggraded in all geomorphic reaches, though 3-TBR was nearly neutral with just 0.86 mm/y of aggradation (Table 4). The wetted areas above the base-flow channel were all erosional, with incision across all geomorphic reaches. Net volumetric changes

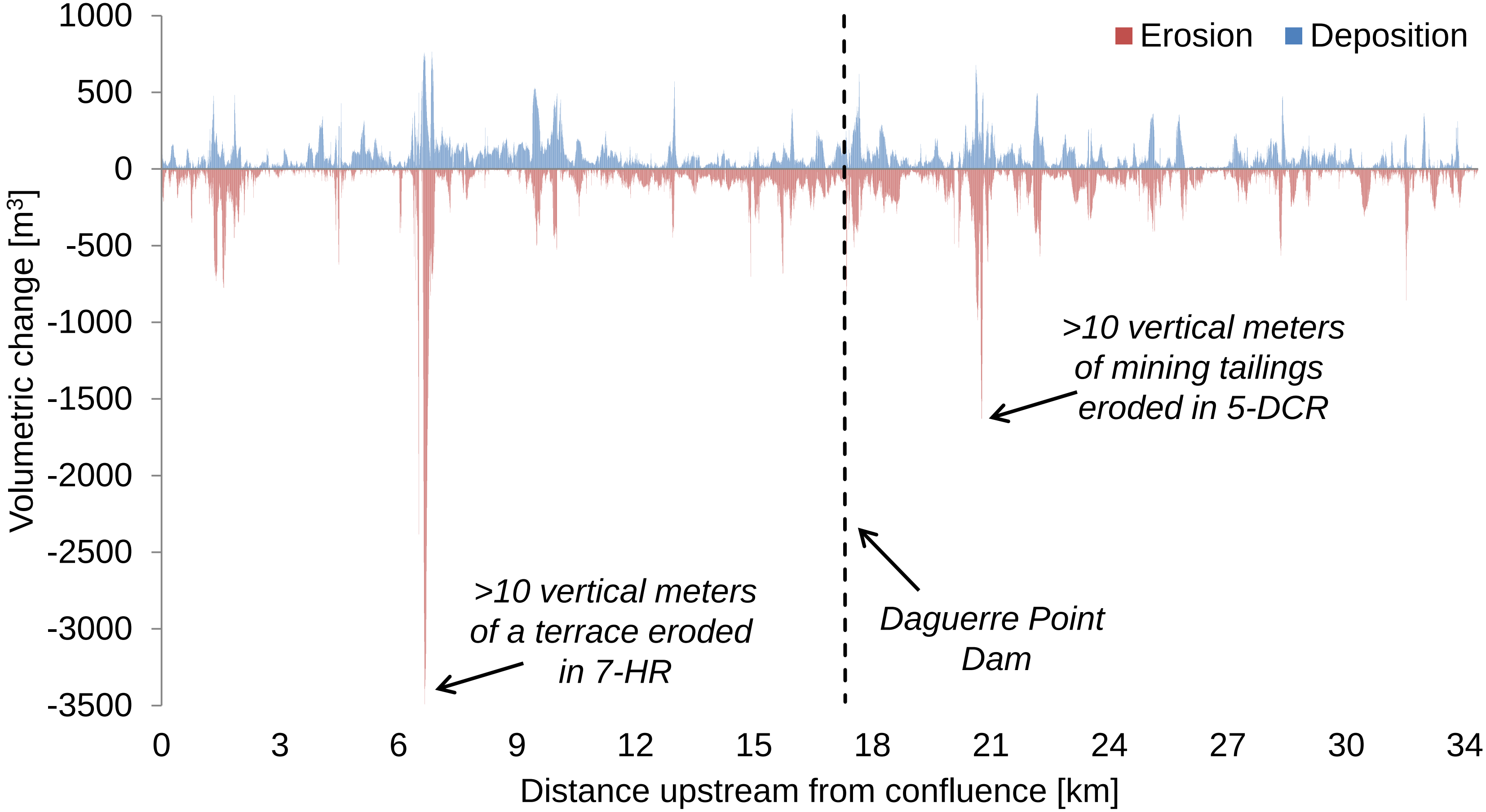

Erosion
Deposition
Volumetric change [m³]
1000
500
0
-500
-1000
-1500
-2000
-2500
-3000
-3500
0
3
6
9
12
15
18
21
24
27
30
34
Distance upstream from confluence [km]
>10 vertical meters of mining tailings eroded in 5-DCR
>10 vertical meters of a terrace eroded in 7-HR
Daguerre Point Dam

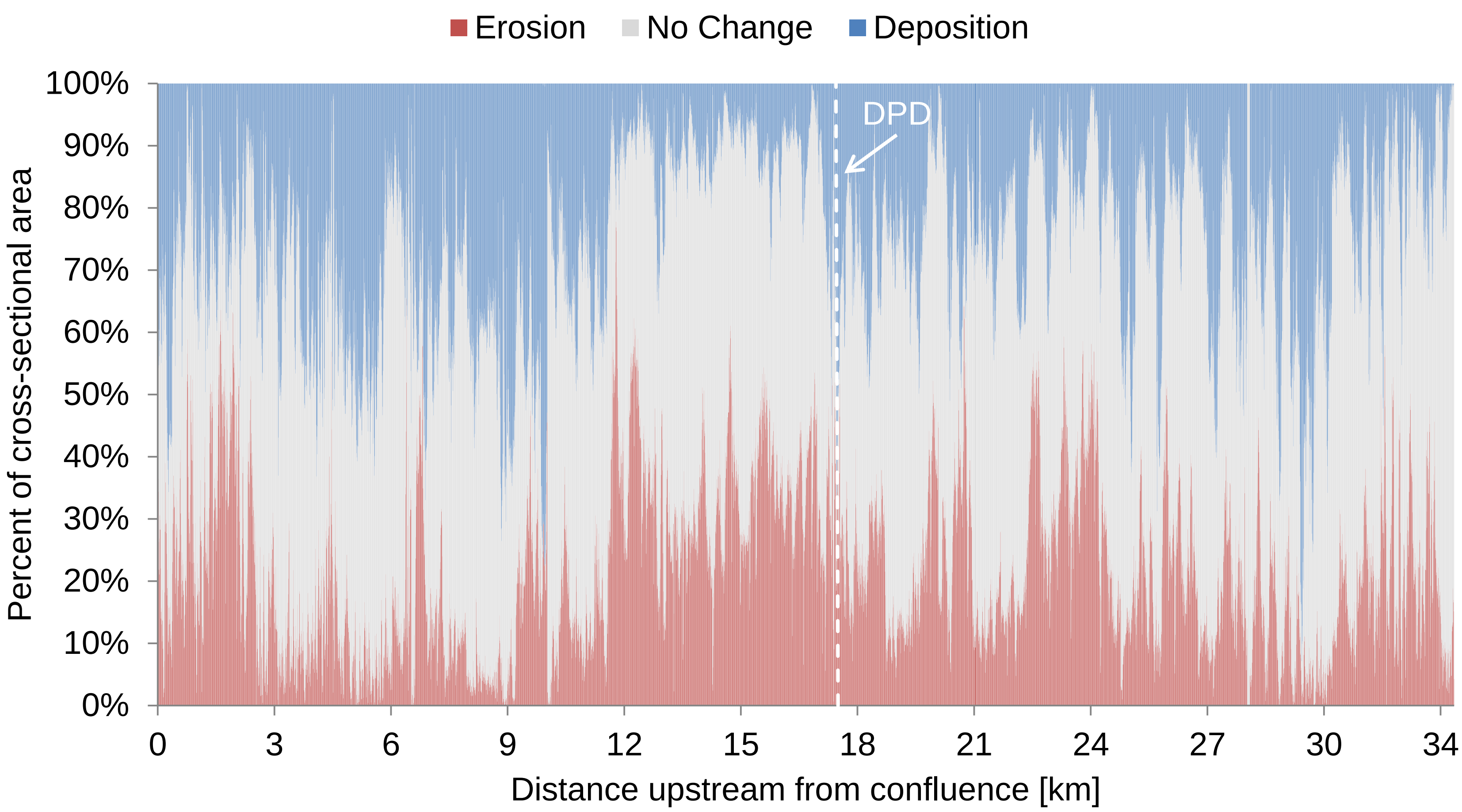

Erosion
No Change
Deposition
DPD
100%
90%
80%
70%
60%
50%
40%
30%
20%
10%
0%
Percent of cross-sectional area
0
3
6
9
12
15
18
21
24
27
30
34
Distance upstream from confluence [km]

Table 3

Volumetric change per year [1000 m^3/y] as separated by in-channel (i.e., bankfull) vs. overbank areas; the numbers reported are the net results within each area (the in-channel vs. overbank analysis was not possible for time period 1; time period 2 is shaded)

	Time period 1	Time period 2		
Reach	Net all	Net in-channel	Net overbank	Net all
3-TBR	-45.0	-0.2	-1.8	-2.0
4-PBR	2.7	0.3	-4.7	-4.4
5-DCR	-57.0	0.5	-6.4	-5.9
6-DPDR	45.0	-0.5	-6.4	-6.9
7-HR	37.0	17.0	-17.0	-0.3
8-MR	0.9	2.4	-5.1	-2.7
All LYR	-17.0	20.0	-42.0	-22.0

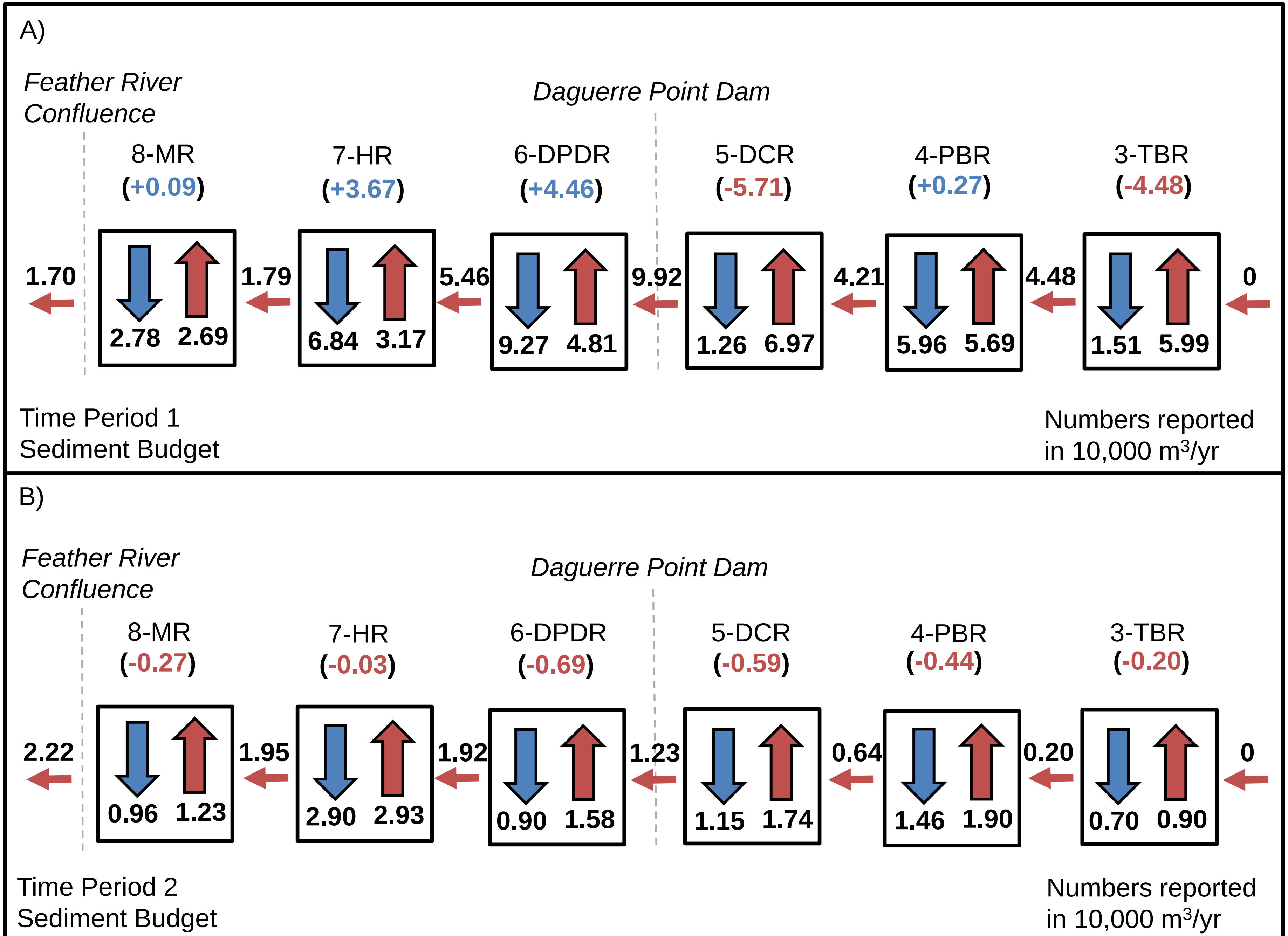
A)
Feather River Confluence
Daguerre Point Dam
8-MR (+0.09)
7-HR (+3.67)
6-DPDR (+4.46)
5-DCR (-5.71)
4-PBR (+0.27)
3-TBR (-4.48)
1.70
2.78 2.69
1.79
6.84 3.17
5.46
9.27 4.81
9.92
1.26 6.97
4.21
5.96 5.69
4.48
1.51 5.99
0
Time Period 1 Sediment Budget
Numbers reported in 10,000 m³/yr
B)
Feather River Confluence
Daguerre Point Dam
8-MR (-0.27)
7-HR (-0.03)
6-DPDR (-0.69)
5-DCR (-0.59)
4-PBR (-0.44)
3-TBR (-0.20)
2.22
0.96 1.23
1.95
2.90 2.93
1.92
0.90 1.58
1.23
1.15 1.74
0.64
1.46 1.90
0.20
0.70 0.90
0
Time Period 2 Sediment Budget
Numbers reported in 10,000 m³/yr

Table 4

Average vertical change per year [mm/y] as analyzed by the incrementally added wetted area for each increase in discharge; the time period averages represent the average vertical change across the entire wetted area of the floodway-filling discharge of 597.5 m^3/s (time period 2 is shaded)

Area	8-MR	7-HR	6-DPDR	5-DCR	4-PBR	3-TBR	All LYR
Time period 1 Avg.	1.0	16.0	19.0	-59.0	1.3	-45.0	-2.5
Base flow	19.0	45.0	6.7	13.0	3.6	0.9	16.0
Bankfull	-29.0	-5.6	-12.0	-15.0	-5.2	-3.8	-9.5
Intermediate	-17.0	-5.9	-3.1	-1.0	-1.4	-2.5	-3.9
Floodway	-25.0	-5.1	-4.6	-7.9	-3.8	-4.1	-6.0
Time period 2 Avg.	-2.3	9.7	-3.1	-1.5	-1.5	-1.5	-1.5

averaged across the 2008 floodway (wetted by 597.5 m^3/s) show minor incision of 1.5-3.1 mm/y for all but 7-HR, which aggraded at 9.7 mm/y during the study period.

4.4. Morphological-Unit Scale

Topographic change results during time period 2 for the 2008 MUs are consistent with observations at the segment and reach scale. Most in-channel base-flow MUs (e.g., runs, fast glides, and pools) were strongly depositional; whereas overbank MUs (e.g., terraces, floodplains, and high floodplains) were strongly erosional (Fig. 9). However, several in-channel bank units were net erosional, including lateral bars (58,000 m^3), banks (12,000 m^3), cutbanks (11,000 m^3), medial bars (6000 m^3), and point bars (4000 m^3). Two in-channel bed MUs were net erosional: slackwaters (7000 m^3) and riffles (2000 m^3). Though within those results, slackwaters, medial bars, point bars, and riffles had similar magnitudes of erosion and deposition.

5. Discussion

5.1. Segment-scale sediment budget differences

The TCD analysis for time period 2 (2006/2008 to 2014) yielded different magnitudes, patterns, and rates of erosion and deposition compared to the TCD reported for time period 1 (1999 to 2006/2008) by Carley et al. (2012). The longitudinal profiles of erosion and deposition show that the locations of each process are more balanced in time period 2 than in time period 1. In time period 2, locations of erosion and deposition were positively correlated with each other. This is typical for patterns of lateral migration, where erosion and deposition occur simultaneously in the same cross section (i.e., erosion at the cutbank and deposition on the point bar). Visual inspection of the TCD

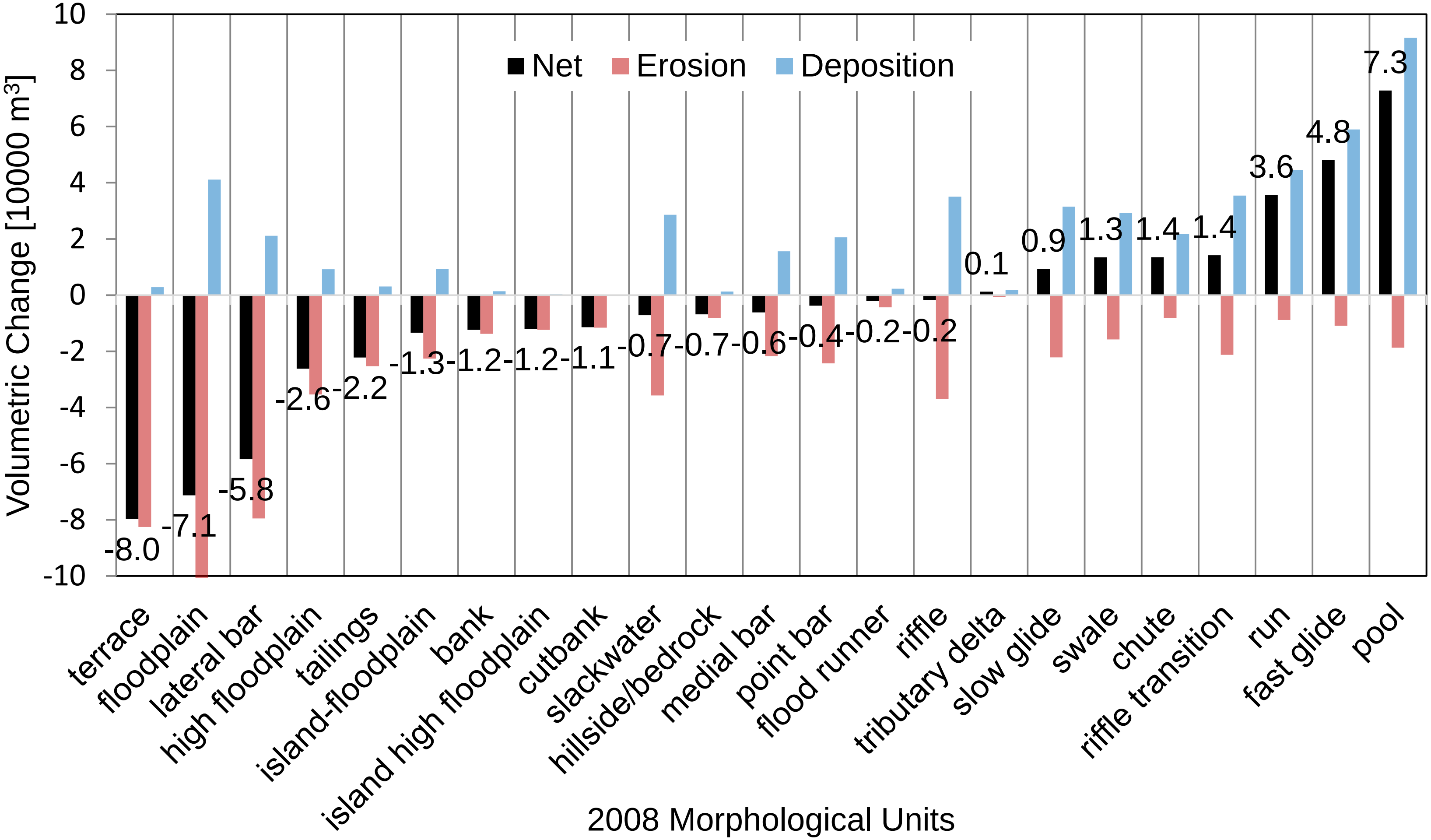

Net
Erosion
Deposition
Volumetric Change [10000 m3]
10
8
6
4
2
0
-2
-4
-6
-8
-10
-8.0
-7.1
-5.8
-2.6
-2.2
-1.3
-1.2
-1.2
-1.1
-0.7
-0.7
-0.6
-0.4
-0.2
-0.2
0.1
0.9
1.3
1.4
1.4
3.6
4.8
7.3
terrace
floodplain
lateral bar
high floodplain
tailings
island-floodplain
bank
island high floodplain
cutbank
slackwater
hillside/bedrock
medial bar
point bar
flood runner
riffle
tributary delta
slow glide
swale
chute
riffle transition
run
fast glide
pool
2008 Morphological Units

raster and local knowledge of the river suggest that eroded material moves a short distance downstream before being deposited. Locations of intense scour were often followed by locations of intense deposition. Thus, in time period 2, sediment was laterally redistributed within LYR with all reaches net erosional, whereas in time period 1, higher flow events caused more vertically dominated processes (e.g., avulsion, overbank scour, and downcutting) that yielded either net erosion or deposition by reach.

Despite the higher flood peaks and longer durations of flood flows during time period 1, the magnitude of net annual export of sediment to the Feather River was similar for the two time periods, with 25% more sediment export during the drought period (time period 2) than during the flood period (17,000 m^3/y in time period 1 vs. 21,300 m^3/y in time period 2). Time period 1 had 20% more days of bankfull flow than time period 2, but it had 25% less net export.

5.2. Reach-scale sediment budget differences

At the reach-scale, erosion and deposition were more imbalanced between the geomorphic reaches for time period 1 than time period 2, with 3-TBR and 5-DCR being strongly erosional and 6-DPDR and 7-HR being strongly depositional. To thoroughly understand this would take an evaluation of the hydraulics during the events in these time periods, but these topographic change patterns correspond well with valley-scale morphological differences. Specifically, we believe that differences in topographic steering between modest vs. large floods are a key contributor to the observed differences in topographic change. Abu-Aly et al. (2014) conducted 2D hydrodynamic flood modeling for LYR (accounting for spatially distributed vegetation roughness), and some of the wetted extents they obtained for relevant flows are provided in Figure 10 to help illustrate the hydraulic mechanism that explains the reach-scale erosion and sedimentation results found in this study.

The two strongly aggradational reaches during time period 1, 6-DPDR and 7-HR, are wider and upstream of 8-MR, which is leveed (Fig. 10C, see zone of constriction). The engineered levees constrict the river corridor in 8-MR by nearly two-thirds (average floodway width decreases from 313 m in 6-DPDR to 116 m in 8-MR). During flood events, this lateral topographic constriction causes water stages to rise higher than they would without the levees, a phenomenon called *levee surcharge* by Heine and Pinter (2012). The levee surcharge would cause a backwater effect upstream of the levees, decrease the water surface slope, and reduce transport capacity. Furthermore, at high discharge, a large secondary channel becomes active within 6-DPDR, creating the widest active floodway within LYR (Fig. 10c, see zone of expansion) and reducing the rate of increase in velocity relative to the other geomorphic reaches (Strom et al., 2016). Together, the flood-stage backwater effect of the levees and the wide floodway in 6-DPDR and 7-HR yield lower flood velocities in these reaches and appear to promote deposition of sediment. Although not part of this study, reach-scale at-a-station hydraulic geometry relations were developed for LYR using 2D hydrodynamic modeling for both in-channel (Gonzalez and Pasternack, 2015) and overbank hydraulics, and the results show reach-scale velocity reversals. First, the mean velocity in 8-MR exceeds that in 7-HR at 212.4 m^3/s, and then it exceeds that in 6-DPDR at 283.2 m^3/s. Above this flow, 8-MR has a significantly higher average velocity than 6-DPDR and 7-HR. In fact, the levees in 8-MR were created to do this by design for the purpose of slowing

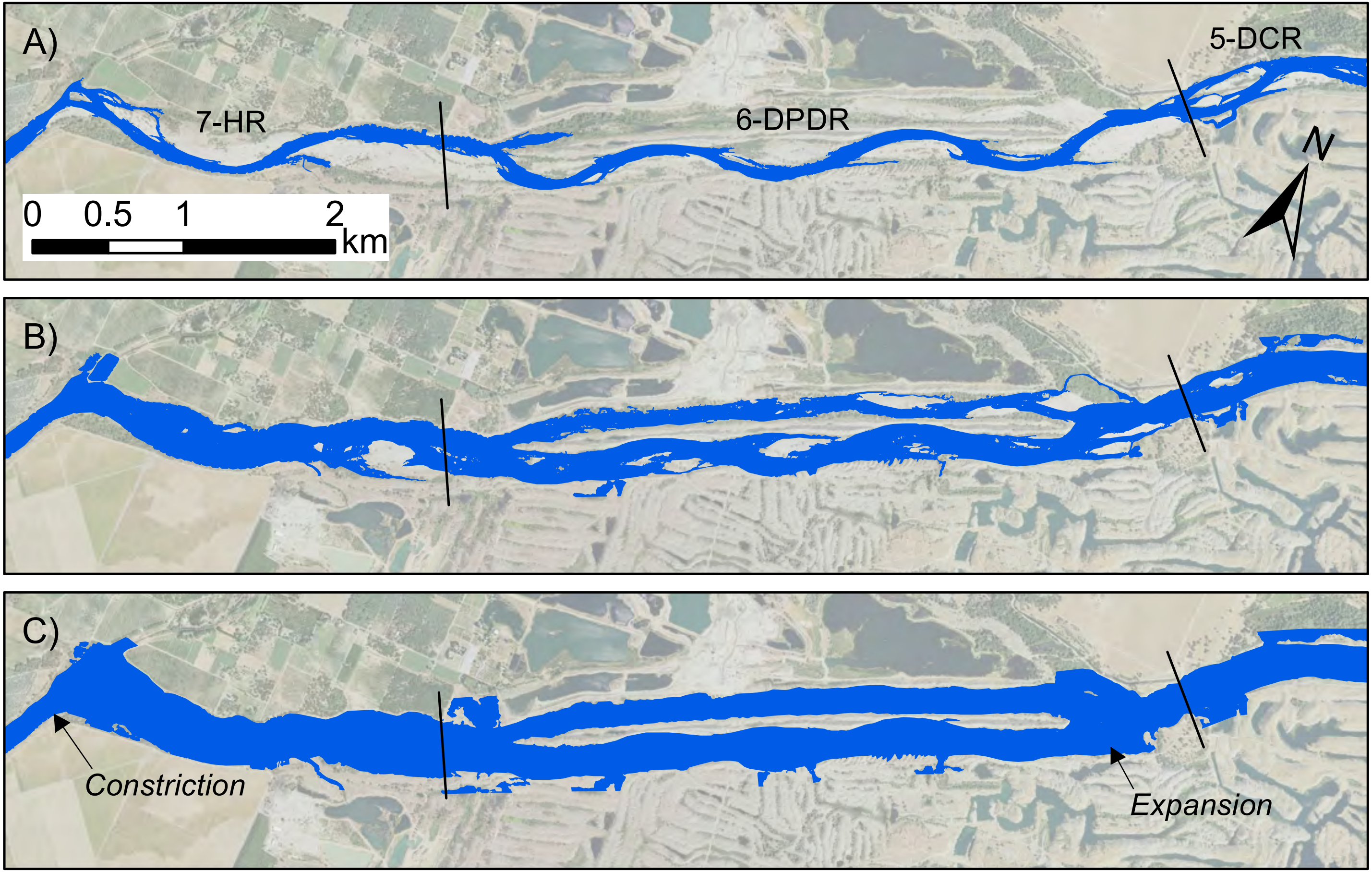
A)
5-DCR
7-HR
6-DPDR
N
0
0.5
1
2
km
B)
C)
Constriction
Expansion

down the export of LYR hydraulic mining debris to the Feather and Sacramento rivers (Adler, 1980).

In contrast to the dynamics in 6-DPDR, 7-HR, and 8-MR, the reaches that eroded during time period 1, 3-TBR and 5-DCR have the lowest entrenchment ratio (i.e., most entrenched), meaning that flood flows in these reaches are constrained within a narrower floodway. As a result, they have higher reach-average velocities and preferentially scour during floods. Overall, the dominant mechanism at work during time period 1 appears to be driven by valley-scale morphological differences within each reach as large floods activate these hydraulic controls.

Given the smaller floods and a shorter overall duration of floodplain-filling flows during time period 2, the hydraulics would have been less impacted by the valley-scale differences between the geomorphic reaches. Furthermore, even though time period 1 had a significantly longer duration of large flooding, the duration above bankfull was only 20% more in time period 1 than in time period 2. This can explain why lateral channel migration processes dominated in time period 2 and why the erosion and deposition patterns were more balanced between the geomorphic reaches. Specifically, at flows at and just above bankfull flow, erosive forces are focused in the channel and on the banks; whereas, after the water spills onto the floodplain, channel velocity can decline, and the patches of peak velocity shift onto the floodplain (Abu-Aly et al., 2014). Thus, apparently the hydraulics in time period 2 were substantially different than in time period 1, and as a result, the topographic change processes and net export were different. This finding provides an important lesson, that more flow does not always mean more erosion (as assumed by specific stream power analysis and commonly applied in geomorphic studies), because the processes of topographic change are stage dependent.

In addition to the differences in flood magnitudes and their associated topographic change processes, topographic changes during time period 2 may be heavily influenced by what happened in time period 1 and the effect that prior floods had on sediment supply and accommodation space. In time period 1, 6-DPDR was strongly depositional, but in time period 2 it was net erosional. Furthermore, for time period 2, 6-DPDR is one of only two reaches where net erosion occurred within the 2008 bankfull channel, and it is the only reach where erosion was the dominant process by area. During time period 2, the channel and floodplain may have been responding to the previous wave of sediment deposition. This highlights the need for repeat topographic change analyses over many time periods in order to understand the role of antecedent conditions prior to interpreting fluvial topographic change results. Along these lines, a large ~ 34-year flood occurred in 1997, and how this changed the distribution of sediment in the river segment is not known. However, it certainly would have established conditions that would influence the results of the 1999 to 2006/2008 TCD analysis.

5.3. Incision rates

Average vertical change rates for time period 1 and time period 2 were similar with 2.4 mm/y of incision for time period 1 and 1.5-3.1 mm/y of incision for time period 2. Although the average values were similar, results at the reach scale were significantly different, with reaches during time period 1 aggrading by as much as 19 mm/y (6-DPDR) and incising by as much as 69 mm/y (5-DCR).

The analysis of vertical change by inundation threshold for time period 2 showed that, while each geomorphic reach was net erosional, incision rates were low (~1.5 to 3.1 mm/y) for the floodway corridor. Furthermore, the base-flow channel aggraded across all geomorphic reaches, whereas the incrementally added wetted areas above base-flow discharge eroded for all geomorphic reaches across all higher discharges. This result further confirms that even as LYR continues to slowly incise, the river is staying well connected to its current floodplain through lateral migration.

The vertical change results for 7-HR may appear to be contradictory as net erosion was calculated for the reach (310 m^3/y), while 9.1 mm/y of aggradation occurred during time period 2 for the 2008 floodway area. This is because of a large bank collapse that eroded a terrace outside of the 2008 floodway (Fig. 5B). Thus, a large amount of erosion occurred outside of the 2008 floodway as the river migrated laterally and deposited material within the former channel. Events like this occurred in several other locations, such as in 5-DCR, where the river eroded into tailings of hydraulic mining debris.

5.4. Sources and sinks of sediment

The bulk of the sediment eroded within LYR between 2006/2008 and 2014 came from three MUs: floodplain (112,000 m^3), terraces (82,600 m^3), and in-channel lateral bars (79,500 m^3). A smaller but significant amount of sediment came from riffles (36,700 m^3), slackwater (35,700 m^3), high floodplain (35,400 m^3), and tailing (25,300 m^3) MUs. The sediment sourced from terraces, high floodplains, and tailings represent landforms that are outside of the 2008 floodway but are being reincorporated into the active river valley as the river migrates. This analysis shows that these landforms higher on the landscape can be a significant component of the sediment dynamics within LYR, with 26% of the sediment being sourced outside of the floodway during time period 2. At the same time, the results continue to support the conclusion that the floodplain and channel are the dominant sources of sediment, even though tailings and terraces produce more visible patterns of topographic change.

5.5. Contrast with other regulated gravel/cobble rivers

Typically, rivers that incise abandon their floodplains. This study presents an uncommon case where the river is incising and evacuating sediment while maintaining channel-floodplain connectivity. In some places along the river, such as in 7-HR and 5-DCR, the extent of the floodplain expanded as the river migrated laterally into former terraces and mining tailings. Historically, LYR did incise and abandon its floodplain in some places, as evident by the presence of intermittent terraces; but from 1999 to 2014, the flood flows and sediment regime remain well connected to the existing floodplain. In time period 1, the sediment connectivity was largely through overbank scour and avulsion; whereas, in time period 2, the connectivity was largely through lateral channel migration.

The LYR, despite being a regulated river, has been able to resist significant, interdecadal bed armoring because of an abundance of alluvium and a heterogeneous flow regime that diversifies its sediment transport mechanisms (Parker et al., 2003). Both time periods found that sediment was preferentially scoured from the floodplain and deposited within the former channel. This redistribution of sediment prevents the persistence of an armored layer. The abundant alluvial fill within the floodway consists of a variety of sediment sizes, with about 10-20% fine gravel [2-32 mm], 20-40% small cobble [32-90 mm], 20-30% cobble [90-128 mm], and 10-20% large cobble [128-256 mm] (Jackson et al., 2013). Furthermore, as LYR migrates laterally and erodes terraces and mining tailings, new material is added to the floodway. Terrace sediments are poorly sorted and consist of sands, gravels, and cobbles (Jackson et al., 2013).

6. Conclusions

This study provided insights into how sediment budgets and incision/aggradation rates differ within LYR during two contrasting decadal flow regimes. During the large flood events of time period 1, sediment within LYR was displaced longitudinally, with reaches above DPD eroding sediment and reaches below DPD accumulating sediment. This finding corresponds with the valley-scale morphological features that are activated at high river stages, such as the levees in 8-MR and 7-HR, the secondary bypass channel in 6-DPDR, and the narrow valley walls in 3-TBR. These valley-scale morphological features drive the hydraulics and sediment movement within LYR at high flow. During the modest floods of time period 2, from 2006/2008 to 2014, the majority of the sediment was laterally redistributed with erosion outside of the base-flow channel (e.g., floodplain, terrace, and lateral bar MUs) and deposition within the former base-flow channel (e.g., pools, runs, and fast glide MUs) as the river channel migrates. The results from 6-DPDR during time period 2 suggest that the previous wave of sediment deposition in that reach influenced the type of topographic change processes that occurred. This finding highlights the need for repeat topographic change studies to understand antecedent conditions and interpret the results. Modern day incision rates averaged across the entire floodway were ~2.5 mm/y for time period 1 and 1.5 mm/y for time period 2. These incision rates are significantly slower than the 6.4 cm/y previously reported by Adler (1980) from 1912 to 1979. Overall, this paper presents the complexities of a gravel/cobble river that experiences vastly different morphodynamics based on the interaction of a dynamic flood regime and multiple layers of topographic heterogeneity.

Acknowledgements

Primary support for this study was provided by the Yuba County Water Agency (Award #201016094) and as in-kind aid from the Yuba Accord River Management Team. This project was also supported by the USDA National Institute of Food and Agriculture, Hatch project number #CA-D-LAW-7034-H. We thank professors Nicholas Pinter and Christophe Hauer for reviews of a draft of the manuscript. We thank Duane Massa, Loren Stearman, Michael Strom, and Scott Burman for help with ground and boat based surveying. We thank Oriane Taft, Mousa Diabat and the other staff from Quantum Spatial with help collecting and processing LiDAR data in 2014. We thank Cody Carlson and the staff at Seafloor Systems for help with collecting multi-beam data in 2014. We thank four anonymous peer reviewers and the editor for revision suggestions and mark-ups that improved the manuscript.

References

Abu-Aly, T.R., Pasternack, G.B., Wyrick, J.R., Barker, R., Massa, D., Johnson, T., 2014. Effects of lidar-derived, spatially distributed vegetation roughness on two-dimensional hydraulics in a gravel-cobble river at flows of 0.2 to 20 times bankfull. Geomorphology, 206, 468-482.

Adler, L.L., 1980. Adjustment of the yuba river, california, to the influx of hydraulic mining debris, 1849-1979. Master of Arts, University of California, Los Angeles, 180 pp.

Arthington, Á.H., Naiman, R.J., Mcclain, M.E., Nilsson, C., 2010. Preserving the biodiversity and ecological services of rivers: New challenges and research opportunities. Freshwater Biology, 55(1), 1-16.

Ashworth, P., Ferguson, R., 1986. Interrelationships of channel processes, changes and sediments in a proglacial braided river. Geografiska Annaler. Series A. Physical Geography, 361-371.

Barker, J.R., 2012. Rapid, abundant velocity observation to validate million-element 2d hydrodynamic models. Master of Science, University of California, Davis.

Boulton, A.J., Fenwick, G.D., Hancock, P.J., Harvey, M.S., 2008. Biodiversity, functional roles and ecosystem services of groundwater invertebrates. Invertebrate Systematics, 22(2), 103-116.

Brasington, J., Vericat, D., Rychkov, I., 2012. Modeling river bed morphology, roughness, and surface sedimentology using high resolution terrestrial laser scanning. Water Resources Research, 48(11).

Brown, R.A., Pasternack, G.B., 2014. Hydrologic and topographic variability modulate channel change in mountain rivers. Journal of Hydrology, 510, 551-564.

Brown, R.A., Pasternack, G.B., 2017. Bed and width oscillations form coherent patterns in a partially confined, regulated gravel–cobble-bedded river adjusting to anthropogenic disturbances. Earth Surface Dynamics, 5(1), 1-20.

Buffington, J.M., Montgomery, D.R., 1999. A procedure for classifying textural facies in gravel-bed rivers. Water Resources Research, 35(6), 1903-1914.

Carbonneau, P., Fonstad, M.A., Marcus, W.A., Dugdale, S.J., 2012. Making riverscapes real. Geomorphology, 137(1), 74-86.

Carley, J.K., Pasternack, G.B., Wyrick, J.R., Barker, J.R., Bratovich, P.M., Massa, D.A., Reedy, G.D., Johnson, T.R., 2012. Significant decadal channel change 58–67years post-dam accounting for uncertainty in topographic change detection between contour maps and point cloud models. Geomorphology, 179, 71-88.

Casado, M.R., Gonzalez, R.B., Kriechbaumer, T., Veal, A., 2015. Automated identification of river hydromorphological features using uav high resolution aerial imagery. Sensors, 15(11), 27969-27989.

Edson, C., Wing, M.G., 2015. Lidar elevation and dem errors in forested settings. Modern Applied Science, 9(2), 139.

Fonstad, M.A., Dietrich, J.T., Courville, B.C., Jensen, J.L., Carbonneau, P.E., 2013. Topographic structure from motion: A new development in photogrammetric measurement. Earth Surface Processes and Landforms, 38(4), 421-430.

Gangodagamage, C., Barnes, E., Foufoula-Georgiou, E., 2007. Scaling in river corridor widths depicts organization in valley morphology. Geomorphology, 91(3), 198-215.

Gilbert, G.K., 1917. Hydraulic-mining debris in the sierra nevada. In: U.S.G. Survey (Ed.).

Gonzalez, R.L., Pasternack, G.B., 2015. Reenvisioning cross-sectional at-a-station hydraulic geometry as spatially explicit hydraulic topography. Geomorphology, 246, 394-406.

Gould, S.B., Glenn, N.F., Sankey, T.T., Mcnamara, J.P., Spaete, L.R., 2013. Influence of a dense, low-height shrub species on the accuracy of a lidar-derived dem. Photogrammetric Engineering and Remote Sensing, 79(5), 421-431.

Hancock, P.J., 2002. Human impacts on the stream–groundwater exchange zone. Environmental management, 29(6), 763-781.

Hazel, J.E., Grams, P.E., Schmidt, J.C., Kaplinski, M., 2010. Sandbar response in marble and grand canyons, arizona, following the 2008 high-flow experiment on the colorado river. 2328-0328, US Geological Survey.

Heine, R.A., Pinter, N., 2012. Levee effects upon flood levels: An empirical assessment. Hydrological Processes, 26(21), 3225-3240.

Hensleigh, J., 2014. Geomorphic change detection using multi-beam sonar. Master of Science, Utah State University, 122 pp.

Heritage, G.L., Milan, D.J., Large, A.R.G., Fuller, I.C., 2009. Influence of survey strategy and interpolation model on dem quality. Geomorphology, 112(3-4), 334-344.

Hilldale, R.C., Raff, D., 2008. Assessing the ability of airborne lidar to map river bathymetry. Earth Surface Processes and Landforms, 33(5), 773-783.

Hodgson, M.E., Bresnahan, P., 2004. Accuracy of airborne lidar-derived elevation: Empirical assessment and error budget. Photogrammetric Engineering and Remote Sensing, 70(3), 331-339.

Jackson, J., Pasternack, G., Wyrick, J., 2013. Substrate of the lower yuba river, Prepared for the Yuba Accord River Management Team, University of California, Davis. , Davis, CA.

James, L.A., 2005. Sediment from hydraulic mining detained by englebright and small dams in the yuba basin. Geomorphology, 71(1-2), 202-226.

James, L.A., Singer, M.B., Ghoshal, S., Megison, M., 2009. Historical channel changes in the lower yuba and feather rivers, california: Long-term effects of contrasting river-management strategies. In: L.A. James, S.L. Rathburn, G.R. Whittecar (Eds.), Management and restoration of fluvial systems with broad historical changes and human impacts. Geological society of america special papers, pp. 57-81.

Javernick, L., Brasington, J., Caruso, B., 2014. Modeling the topography of shallow braided rivers using structure-from-motion photogrammetry. Geomorphology, 213, 166-182.

Kleinhans, M.G., 2010. Sorting out river channel patterns. Progress in Physical Geography, 34(3), 287-326.

Kraus, K., Karel, W., Briese, C., Mandlburger, G., 2006. Local accuracy measures for digital terrain models. Photogrammetric Record, 21(116), 342-354.

Lane, S.N., Westaway, R.M., Murray Hicks, D., 2003. Estimation of erosion and deposition volumes in a large, gravel-bed, braided river using synoptic remote sensing. Earth Surface Processes and Landforms, 28(3), 249-271.

Legleiter, C.J., Roberts, D.A., Lawrence, R.L., 2009. Spectrally based remote sensing of river bathymetry. Earth Surface Processes and Landforms, 34(8), 1039-1059.

Liébault, F., Piégay, H., 2001. Assessment of channel changes due to long-term bedload supply decrease, roubion river, france. Geomorphology, 36(3), 167-186.

Ligon, F.K., Dietrich, W.E., Trush, W.J., 1995. Downstream ecological effects of dams. Bioscience, 45(3), 183-192.

Lindsay, J.B., Ashmore, P.E., 2002. The effects of survey frequency on estimates of scour and fill in a braided river model. Earth Surface Processes and Landforms, 27(1), 27-43.

Lisle, T.E., Church, M., 2002. Sediment transport-storage relations for degrading, gravel bed channels. Water Resources Research, 38(11).

Macwilliams, M.L., Wheaton, J.M., Pasternack, G.B., Kitinidis, P.K., Street, R.L., 2006. The flow convergence-routing hypothesis for pool-riffle maintenance in alluvial rivers. Water Resources Research, 42(W10427), doi:10.1029/2005WR004391.

Mandlburger, G., Hauer, C., Wieser, M., Pfeifer, N., 2015. Topo-bathymetric lidar for monitoring river morphodynamics and instream habitats-a case study at the pielach river. Remote Sensing, 7(5), 6160-6195.

Marquis, G.A., Roy, A.G., 2012. Using multiple bed load measurements: Toward the identification of bed dilation and contraction in gravel-bed rivers. Journal of Geophysical Research: Earth Surface, 117(F1), F01014.

Merz, J.E., Pasternack, G.B., Wheaton, J.M., 2006. Sediment budget for salmonid spawning habitat rehabilitation in the mokelumne river. Geomorphology, 76(1-2), 207-228.

Milan, D.J., Heritage, G.L., Large, A.R.G., Fuller, I.C., 2011. Filtering spatial error from dems: Implications for morphological change estimation. Geomorphology, 125(1), 160-171.

Millar, R.G., 2005. Theoretical regime equations for mobile gravel-bed rivers with stable banks. Geomorphology, 64(3), 207-220.

Nicholas, A., Ashworth, P., Sambrook Smith, G., Sandbach, S., 2013. Numerical simulation of bar and island morphodynamics in anabranching megarivers. Journal of Geophysical Research: Earth Surface, 118(4), 2019-2044.

Oorschot, M.V., Kleinhans, M., Geerling, G., Middelkoop, H., 2015. Distinct patterns of interaction between vegetation and morphodynamics. Earth Surface Processes and Landforms.

Parker, G., 1979. Hydraulic geometry of active gravel rivers. Journal of the Hydraulics Division, 105(9), 1185-1201.

Parker, G., Toro-Escobar, C.M., Ramey, M., Beck, S., 2003. The effect of floodwater extraction on the morphology of mountain streams. Journal of Hydraulic Engineering, 129(11), 885-895.

Passalacqua, P., Belmont, P., Staley, D.M., Simley, J.D., Arrowsmith, J.R., Bode, C.A., Crosby, C., Delong, S.B., Glenn, N.F., Kelly, S.A., Lague, D., Sangireddy, H., Schaffrath, K., Tarboton, D.G., Wasklewicz, T., Wheaton, J.M., 2015. Analyzing

high resolution topography for advancing the understanding of mass and energy transfer through landscapes: A review. Earth-Science Reviews, 148, 174-193.
Pasternack, G.B., Tu, D., Wyrick, J., 2014. Chinook adult spawning physical habitat of the lower yuba river, Prepared for the Yuba Accord River Management Team. University of California, Davis, Davis, CA.
Pasternack, G.B., Wyrick, J.R., 2016. Flood-driven topographic changes in a gravel-cobble river over segment, reach, and morphological unit scales. Earth Surface Processes and Landforms, doi: 10.1002/esp.4064.
Reutebuch, S.E., Mcgaughey, R.J., Andersen, H.E., Carson, W.W., 2003. Accuracy of a high-resolution lidar terrain model under a conifer forest canopy. Canadian Journal of Remote Sensing, 29(5), 527-535.
Shen, H., Schumm, S., Nelson, J., Doehring, D., Skinner, M., 1981. Methods for assessment of stream-related hazards to highways and bridges.
Snyder, N.P., Rubin, D.M., Alpers, C.N., Childs, J.R., Curtis, J.A., Flint, L.E., Wright, S.A., 2004. Estimating accumulation rates and physical properties of sediment behind a dam: Englebright Lake, Yuba River, northern california. Water Resources Research, 40(11), 1-19.
Snyder, N.P., Wright, S.A., Alpers, C.N., Flint, L.E., Holmes, C.W., Rubin, D.M., 2006. Reconstructing depositional processes and history from reservoir stratigraphy: Englebright lake, yuba river, northern california. J. Geophys. Res.-Earth Surf., 111(F4).
Strom, M.A., Pasternack, G.B., Wyrick, J.R., 2016. Reenvisioning velocity reversal as a diversity of hydraulic patch behaviors. Hydrological Processes, 30, 2348–2365.
Tal, M., Paola, C., 2010. Effects of vegetation on channel morphodynamics: Results and insights from laboratory experiments. Earth Surface Processes and Landforms, 35(9), 1014-1028.
Tinkham, W.T., Hoffman, C.M., Falkowski, M.J., Smith, A.M.S., Marshall, H.P., Link, T.E., 2013. A methodology to characterize vertical accuracies in lidar-derived products at landscape scales. Photogrammetric Engineering and Remote Sensing, 79(8), 709-716.
Vericat, D., Smith, M.W., Brasington, J., 2014. Patterns of topographic change in sub-humid badlands determined by high resolution multi-temporal topographic surveys. Catena, 120, 164-176.
Wechsler, S.P., Kroll, C.N., 2006. Quantifying dem uncertainty and its effect on topographic parameters. Photogrammetric Engineering and Remote Sensing, 72(9), 1081-1090.
Westoby, M.J., Brasington, J., Glasser, N.F., Hambrey, M.J., Reynolds, J.M., 2012. 'Structure-from-motion' photogrammetry: A low-cost, effective tool for geoscience applications. Geomorphology, 179, 300-314.
Wheaton, J.M., Darby, S.E., Sear, D.A., 2008. The scope of uncertainties in river restoration, River restoration: Managing the uncertainty in restoring physical habitat, pp. 21-39.
Wheaton, J.M., Brasington, J., Darby, S.E., Sear, D.A., 2010. Accounting for uncertainty in dems from repeat topographic surveys: Improved sediment budgets. Earth Surface Processes and Landforms, 35(2), 136-156.

Wheaton, J.M., Brasington, J., Darby, S.E., Kasprak, A., Sear, D., Vericat, D., 2013. Morphodynamic signatures of braiding mechanisms as expressed through change in sediment storage in a gravel-bed river. J. Geophys. Res.-Earth Surf., 118(2), 759-779.Wheaton, J.M., Fryirs, K.A., Brierley, G., Bangen, S.G., Bouwes, N., O'brien, G., 2015. Geomorphic mapping and taxonomy of fluvial landforms. Geomorphology, 248, 273-295.

White, J.Q., Pasternack, G.B., Moir, H.J., 2010. Valley width variation influences riffle-pool location and persistence on a rapidly incising gravel-bed river. Geomorphology, 121(3-4), 206-221.

Wilcock, P.R., 1997. The components of fractional transport rate. Water Resources Research, 33(1), 247-258.

Wilkinson, S.N., Rutherfurd, I.D., Keller, R.J., 2008. An experimental test of whether bar instability contributes to the formation, periodicity and maintenance of pool-riffle sequences. Earth Surf. Processes Landforms, 33, 1742-1756.

Williams, R.D., Brasington, J., Vericat, D., Hicks, D.M., 2014. Hyperscale terrain modelling of braided rivers: Fusing mobile terrestrial laser scanning and optical bathymetric mapping. Earth Surface Processes and Landforms, 39(2), 167-183.

Wu, F.C., Yeh, T.H., 2005. Forced bars induced by variations of channel width: Implications for incipient bifurcation. Jounal of Geophysical Research, 110(F02009), doi:10.1029/2004JF000160.

Wyrick, J.R., Pasternack, G.B., 2012. Landforms of the lower yuba river, University of California, Davis, CA.

Wyrick, J.R., Pasternack, G.B., 2014. Geospatial organization of fluvial landforms in a gravel-cobble river: Beyond the riffle-pool couplet. Geomorphology, 213, 48-65.

Wyrick, J.R., Pasternack, G.B., 2015. Revealing the natural complexity of topographic change processes through repeat surveys and decision-tree classification. Earth Surface Processes and Landforms, 41(6), 723-737. doi: 10.1002/esp.3854..

Wyrick, J.R., Senter, A.E., Pasternack, G.B., 2014. Revealing the natural complexity of fluvial morphology through 2d hydrodynamic delineation of river landforms. Geomorphology, 210, 14-22.

Figure Captions

Fig. 1. Site map of the lower Yuba River (LYR) in northern California. The grey area in the bottom map depicts the estimated inundated area for a flow of 1195 m^3/s. LYR begins at the downstream end of Englebright Dam and continues until its confluence with the Feather River.

Fig. 2. Longitudinal profile of the 2014 bed elevation along the thalweg for the lower Yuba River with geomorphic reaches delineated. Elevations were derived from bathymetric LiDAR and multibeam sonar data with respect to NAVD88.

Fig. 3. Instantaneous flow hydrograph for time period 1 (1999-2006/2008) and time period 2 (2006/2008-2014) for LYR at the Marysville USGS gage (11421000). Time period 2 is shaded.

Fig. 4. Example outputs from the DEM uncertainty and TCD analysis using the 2014 data. (A) 2014 aerial photo. (B) 2014 raster DEM. (C) 2014 land cover raster. (D) 2014 point density raster. (E) 2014 SD_Z raster. (F) 2014 SEM raster. (G) 2008-2014 LOD95 raster. (H) Raw topographic change results. (I) Statistically significant topographic change results.

Fig. 5. (A) Example of TCD results in the Hallwood Reach, where lateral migration caused the collapse of a forested terrace and orchard with >10 m of vertical scour. Deposition primarily occurred within the 2008 base-flow channel. (B) Map of wetted areas produced by a 2D hydrodynamic model. The location of scour outside the floodway demonstrates how the river expanded its active floodway in

this stretch by eroding a terrace. (C) Map of the 2008 MUs delineated by Wyrick and Pasternack (2012, 2014).

Fig. 6. Longitudinal series of deposition and erosion volumes in the lower Yuba River valley for the 2006/2008 to 2014 time period.

Fig. 7. Longitudinal series of deposition and erosion as a percentage of the floodway area for the 2006/2008 to 2014 time period. On average, 22% of the floodway experienced erosion, 25% deposition, and 53% did not change, though significant variation exists among the geomorphic reaches.

Fig. 8. Sediment budget by geomorphic reach for time period 1 (A) and time period 2 (B). The numbers are reported as volumetric rates in 10,000 m^3/y. Each geomorphic reach is presented as a control volume with their inputs and exports of sediment shown by the horizontal arrows. The net change in sediment storage for each reach is shown in parentheses below the reach label, where positive values indicate net deposition and negative values indicate net erosion. Within each reach, the downward arrows indicate the gross rates of deposition and the upward arrows indicate the gross rates of erosion within each reach. The value left of the Feather River confluence marker is the average annual volume of sediment exported out of the LYR valley to the Feather River.

Fig. 9. Volumetric change within the 2006/2008 morphological unit delineations during time period 2. The black bars and data labels show the net volumetric change in 10,000 m^3.

Fig. 10. The panels show wetted extents from Abu-Aly et al. (2014) for three different discharges. The lines show geomorphic reach breaks with reach labels in panel

A. (A) Wetted extent for bankfull discharge (141.6 m^3/s). (B) Wetted extent for the floodway filling discharge (597.5 m^3/s), which is approximately the peak daily-averaged flow for time period 2. Notice that the sinuosity of the base-flow channel is still apparent in the wetted extent for this discharge, indicating that the bankfull channel is still steering the hydraulics. (C) Wetted extent for 2390 m^3/s, which is approximately the peak daily-averaged flow for time period 1. Notice that the sinuosity of the base-flow channel is no longer visible in the wetted extent for this discharge. Instead, expansion and contraction of the wetted extent occurs at multiple scales. An overall zone of expansion begins just below the entrance of 6-DPDR, where the floodway splits in two. Then, an overall contraction occurs at the downstream end of the figure in 7-HR, where the wetted width more than halves. In addition, multiple smaller scale expansion and contractions occur throughout this section of river.

Supplementary Materials

Valley-scale morphology drives differences in fluvial sediment budgets and incision rates during contrasting flow regimes

Matthew David Weber

Gregory Brian Pasternack*

University of California, Davis, One Shields Avenue, Davis, CA 95616, USA

* Corresponding author. Tel.: +1 (530) 302-5658

E-mail: gpast@ucdavis.edu

Contents of this file

S1. Introduction

The supplementary materials provide information on the lower Yuba River's geomorphic reaches (Section S2.1) and morphological units (Section S2.2), the topographic data collection efforts for the 2006/2008 topographic map (Section S4.1) and the 2014 topographic map (Section S4.2), the DEM uncertainty method (Section S5.1), and cross-section boxes used to aggregate results (Section S5.1). In addition, overview maps of the 2006/2008 – 2014 topographic change results are presented in a separate PDF.

S2. Study site – Lower Yuba River Supplements

S2.1. Geomorphic Reaches

The six alluvial geomorphic reaches of LYR discussed in this study are Timbuctoo Bend Reach (3-TBR), Parks Bar Reach (4-PBR), Deer Creek Reach (5-DCR), Daguerre Point Dam Reach (6-DPDR), Hallwood Reach (7-HR), and Marysville Reach (8-MR). 3-TBR begins 34.0 river kilometers (RKm) upstream from the confluence with the Feather River. 3-TBR marks the emergence of a gravel/cobble floodplain as the river transitions from a narrow bedrock canyon to a wider bedrock valley with some river meandering. In 4-PBR (21.3-28.3 RKm), the river valley width nearly doubles as the river enters a broad alluvial valley with few locations of bedrock controls. The Dry Creek Reach (5-DCR) begins where Dry Creek, an ungaged tributary, enters LYR at RKm 21.3. The bed slope significantly decreases in 5-DCR (from 0.0019 in 4-PBR to 0.0014 in 5-DCR), which is associated with the backwater effects from Daguerre Point Dam (DPD). 6-DPDR begins downstream of DPD (RKm 17.8). It has the widest active valley with a secondary channel (i.e., flood runner) that is occupied with water when flows reach above 330 m^3/s. 7-HR marks another slope break (from 0.0018 in 6-DPDR to 0.0013 in 7-HR), and the river corridor begins to be laterally constricted from levees. The last geomorphic reach is the Marysville Reach (8-MR), which is defined by a very low bed slope (0.0005) and backwater effects from the Feather River. It is laterally constricted and heavily channelized from levees that protect the City of Marysville. A summary of geomorphic reach statistics is provided in Table S1.

Table S1. Geomorphic reach metrics for the alluvial lower Yuba River

Reach	Mean Bankfull Width [m]	Mean Floodway Width [m]	Entrench-ment Ratio	Width:Depth Ratio	Sinuosity	Slope	Substrate d_{50} [mm]
3-TBR	84.4	134.4	2.12	82.4	1.10	0.0020	164
4-PBR	96.3	206.7	2.93	107.9	1.14	0.0019	117
5-DCR	130.1	263.7	2.45	122.3	1.06	0.0014	87
6-DPDR	119.8	313.3	3.54	85.4	1.13	0.0018	87
7-HR	102.1	210.9	2.61	70.8	1.08	0.0013	61
8-MR	70.4	115.5	2.61	23.1	1.07	0.0005	40

S2.2. Morphological Units

Morphological Units (MUs) are river landforms mapped at the scale of ~0.1-10 channel widths and are considered the basic building blocks of fluvial morphology (Grant et al., 1990; Wadeson, 1994; Brierley and Fryirs, 2000; Wheaton et al., 2015). Names used in the literature for these discernable units include “physical biotope” (Newson and Newson, 2000), “channel geomorphic unit” (Hawkins et al., 1993), “channel unit” (Grant et al., 1990), and “morphological unit” (Wadeson, 1994).

The MUs delineated for LYR were developed based on the 2006/2008 topographic map and are categorized into four categories: in-channel bed MUs, in-channel bar MUs, floodway MUs, and valley MUs. These categories are segregated by inundation thresholds determined by a 2-dimensional (2D) hydrodynamic model (SRH-2D) with in-channel bed MUs delineated at baseflow discharge (24.92 m^3/s above DPD and 15.01 m^3/s below DPD), in-channel bar MUs delineated within the incrementally added area at bankfull discharge (141.6 m^3/s), floodway MUs delineated within the incrementally added area at the floodway filling discharge (597.5 m^3/s), and valley MUs delineated in areas outside of the floodway. There are eight in-channel bed MUs. The method for delineating these eight MUs was presented in (Wyrick et al., 2014), Fig. S1 shows the combinations of depth and velocity that were used to delineate each MU, and Table S2 provides a qualitative description of each of the in-channel bed MUs. The other categorical MUs were delineated manually in ArcGIS on an expert-basis using information obtained from field surveys, topographic indicators (e.g., slope breaks), and topographic change maps from 1999-2008. Details on this mapping effort was provided in (Wyrick and Pasternack, 2012), Table S3-5 provide qualitative descriptions of each of the MUs, and Fig. S2 provides an example map of the MUs for 4-PBR.

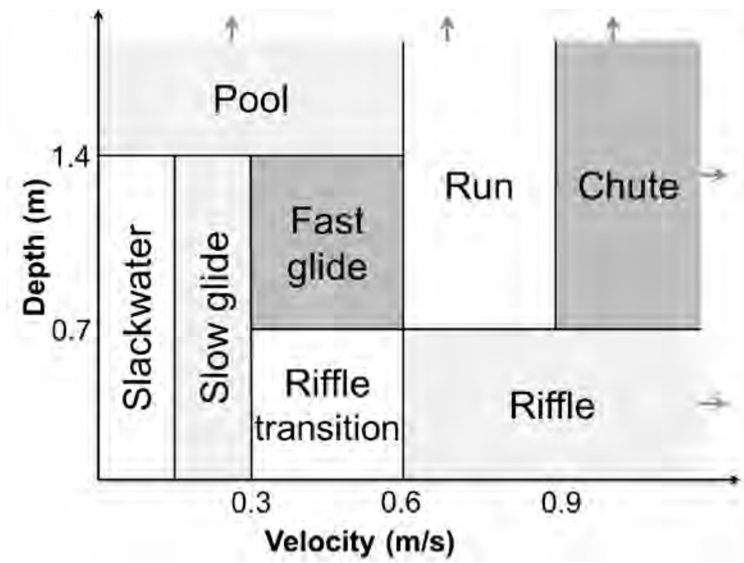

Fig. S1. Combinations of depth and velocity used to delineate in-channel bed morphological units for the lower Yuba River using the outputs of a 2-dimensional hydrodynamic model at baseflow discharge. Reproduced from Wyrick et al. (2014).

Table S2. Qualitative descriptions of in-channel bed morphological units mapped in LYR. Reproduced from Wyrick and Pasternack (2012).

Unit Name	Description
Chute	Area of high velocity, steep water surface slope, and moderate to high depth located in the channel thalweg. Chutes are often located in a convergent constriction downstream of a riffle as it transitions into a run, forced pool, pool, or glide.
Fast Glide	Area of moderate velocity and depth and low water surface slope. Commonly occur along periphery of channel and flanking pools. Also exist in straight sections of low bed slope.
Pool / Forced Pool	Pools are areas of high depth and low velocity, and low water surface slope. The distinction between 'forced pool' and 'pool' cannot be made automatically within GIS. A 'forced pool' is one that is typically along the periphery of the channel and is "over-deepened" from local convective acceleration and scour during floods that is associated with static structures such as wood, boulders, and mostly bedrock outcrops. A 'pool' is not formed by a forcing obstruction.
Riffle	Area with shallow depths, moderate to high velocities, rough water surface texture, and steep water surface slope. Riffles are associated with the crest and backslope of a transverse bar.
Riffle Transition	Typically a transitional area between an upstream morphological unit into a riffle, or from a riffle into a downstream morphological unit. Water depth is relatively low. Velocity is low, but increases downstream due to convective acceleration toward the shallow riffle crest that is caused by lateral and vertical flow convergence. The upstream limit is at the approximate location where there is a transition from a divergent to convergent flow pattern. The downstream limit is at the slope break of the channel bed termed the riffle crest.
Run	Area with a moderate velocity, high depths, and moderate water surface slope. Runs typically occur in straight sections that exhibit a moderate water surface texture and tend not to be located over transverse bars.
Slow Glide	Area of low velocity and low to moderate depths and low water surface slope. May be located near water's edge as a morphological unit along the channel thalweg transitions laterally towards the stream margins.
Slackwater	Shallow, low-velocity regions of the stream that are typically located in adjacent embayments, side channels, or along channel margins. Velocities are near stagnant during baseflow conditions and rise slower than other bed units' as stage increases.

Table S3. Qualitative descriptions of in-channel bar morphological units mapped in LYR. Reproduced from Wyrick and Pasternack (2012).

Unit Name	Description
Lateral Bar	Area located at the channel margins at an elevation band between the autumnal low-flow stage and bankfull stage. Lateral bars are orientated parallel to the flow. The feature slopes toward the channel thalweg with an associated increase in both flow depth and velocity when submerged. Sediment size tends to be smaller than in adjacent sections of the channel.
Medial Bar	Area that is separated from the channel banks at low-flow stages at an elevation band between low-flow and bankfull stages. Can be accreting or eroding.
Point Bar	Accreting area located on the inside of a meander bend at an elevation band between the low-flow stage and bankfull stage. Point bars are curved and begin where there is clear evidence of point-bar deposition. The feature slopes toward the channel thalweg with an associated increase in both flow depth and velocity when submerged. Sediment size tends to be smaller than in adjacent sections of the channel.
Swale	A weakly-defined geometric channel or adjacent bench on the floodplain that only conveys flow at stages above low-flow.
Bridge Pier*	Man-made structural supports for road and rail crossings. Typically composed on concrete and steel. Units also exist at stages above Bankfull flow to a lesser extent.

Table S4. Qualitative descriptions of floodway morphological units mapped in LYR. Reproduced from Wyrick and Pasternack (2012).

Unit Name	Description
Floodplain	Natural alluvium located at an elevation higher than the bankfull channel and lower than the upper wetted extent of the floodway (defined as 21,100 cfs here).
Flood Runner	Relatively straight floodplain channel with uniform geometry and low depths that conveys a concentrated flow at stages above bankfull.
Island-Floodplain	Natural alluvium on a medial bar located at an elevation higher than the bankfull channel and lower than the upper wetted extent of the floodway (defined as 21,100 cfs here).
Mining Pit	Artificial depression created for mining purposes that is adjacent to the flow channel and continuously wetted. May have an artificial connection to floodway channel that is normal to the flow direction.
Backswamp *	Natural depression within the floodplain whose bed elevation intersects with the groundwater table creating a continuously wetted or swampy area. Typically contains vegetation. Units also exist within Bankfull and Valley boundaries to a lesser extent.
Pond*	Natural depression with a continuously measurable depth located on the floodplain and is not attached to the main channel by a surface opening during the low flow at which the in-channel bed morphological units are mapped. Units also exist within Bankfull boundaries to a lesser extent.
Tributary Channel*	Those sections of perennial tributary streams that are located within the bankfull and higher wetted areas of the main channel. Units also exist within Bankfull and Valley boundaries to a lesser extent.
Spur Dike*	Artificial bank protection composed of very large riprap. Usually located along steep banks to prevent further erosion. Units also exist within Bankfull and Valley boundaries to a lesser extent.

Table S5. Qualitative descriptions of morphological units mapped in LYR that are off-channel, but within the active geomorphic valley width. Reproduced from Wyrick and Pasternack (2012).

Unit Name	Description
Terrace	A natural alluvial deposit separated from the floodplain surface by a vertical topographic riser. Terraces are generally abandoned floodplains that have been separated from the channel by vertical incision of lateral migration.
High Floodplain	Natural alluvium located between the terrace riser and the 21,100 cfs wetted area floodplain.
Island-High Floodplain	Natural alluvial deposit on a medial bar located at an elevation higher than the island-floodplain surface.
Levee	Artificially-built flood control berm located parallel to the channel.
Hillside / Bedrock*	Natural colluvium and bedrock at an elevation greater than the valley toe slope break. Units also exist within the Bankfull and Floodway boundaries to a lesser extent.
Bank*	Steep, near-vertical bank that separates bar units from terraces. Gravel/cobble alluvium that line the main channel and not actively experiencing lateral erosion. Units also exist within the Bankfull and Floodway boundaries to a lesser extent.
Cutbank*	Steep, near-vertical bank that separates bar units from terraces. Located on the outside of a meander bend and created by active lateral erosion through local alluvia. Units also exist within the Bankfull and Floodway boundaries to a lesser extent.
Agriplain*	Agriculture field inundated at flows higher than bankfull. These units also exist within the Floodway boundary to a lesser extent.
Tailings*	Steep alluvium artificially piled up adjacent to the channel during historic gold dredging operations. Units also exist within the Bankfull and Floodway boundaries to a lesser extent.
Tributary Delta*	Alluvial fans penetrating the floodplain and main channel at tributary junctions. Units also exist within the Bankfull and Floodway boundaries to a lesser extent.

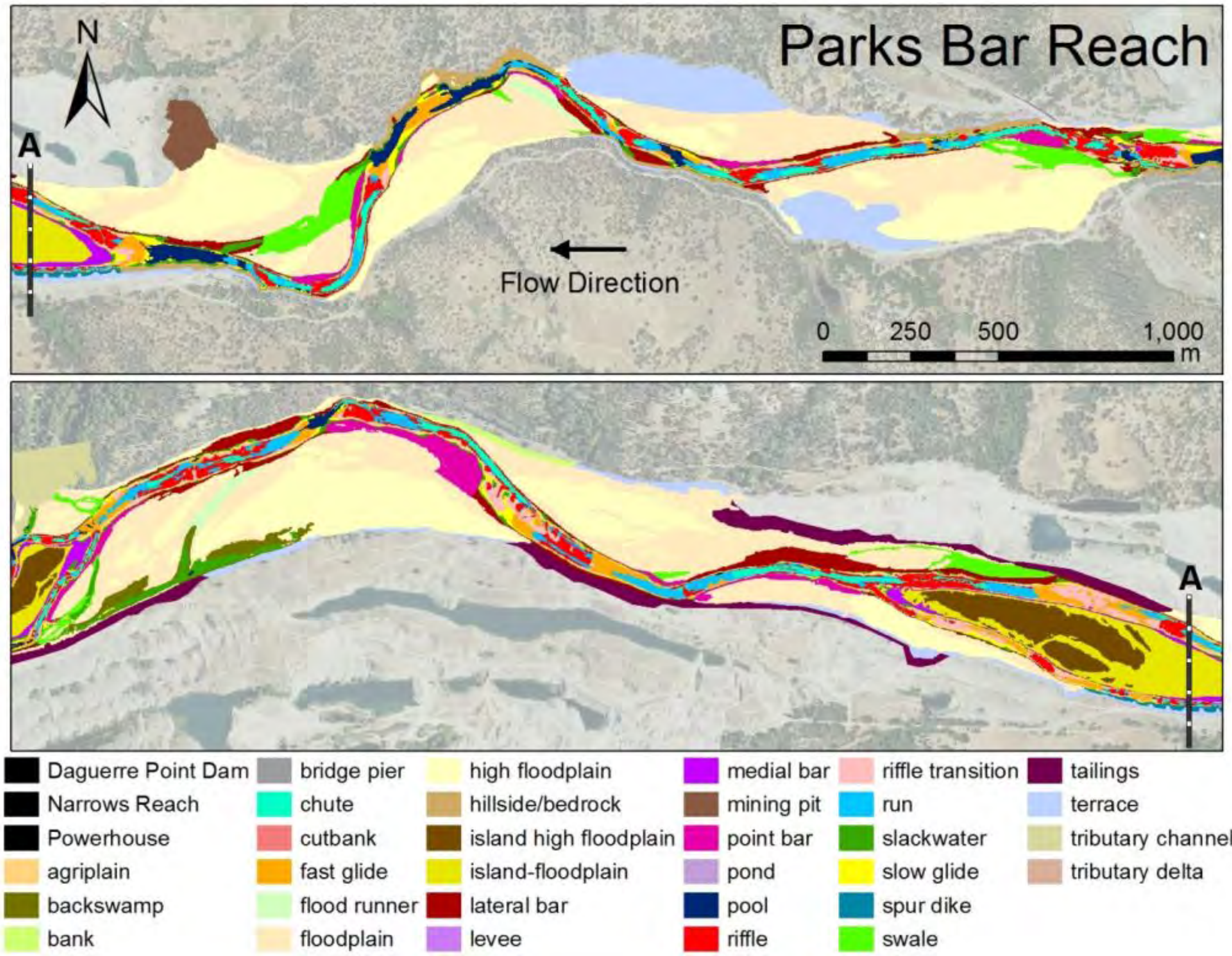

Fig. S2. Morphological unit map within the Parks Bar Reach. Reproduced from Wyrick and Pasternack (2012).

S4. Data

S4.1. 2006/2008 Topographic Map Supplements

S.4.1.1. Data Collection

A 2006/2008 topographic map of the lower Yuba River (LYR) was produced through a phased effort as funding and need permitted. The period between June 2006 and March 2009 was dry with low flows, so it was reasonable to extend mapping over the period to meet project constraints. Data gaps surveyed in November 2009 were shallow backwater, side-channel, and near-bank areas that were unlikely to experience significant change during the modest overbank flows of March and May 2009.

During the dry season of 2006, 3-TBR was mapped using a robotic total station in terrestrial and wadable bathymetric areas. Data was collected in a ~ 3 × 3 m^2 grid in the wetted channel and a ~ 6 × 6 m^2 grid outside of it. For unwadable bathymetry, a professional hydrography firm (Environmental Data Solutions, San Rafael, CA) was contracted to collect bathymetric points along longitudinal and cross-channel lines, meeting the class 1 standard (± 0.15 m vertical accuracy). The topographic and bathymetric procedural details used were explained in Sawyer et al. (2010) for a smaller mapping effort done in 3-TBR in 2005. The overall point spacing for 3-TBR is presented in Table S6.

Downstream of 3-TBR, a mix of LiDAR, single-beam sonar (SBS), total station and RTK-GPS surveys were used to map the river corridor. Aero-Metric, Inc. (Seattle, WA) acquired near-infrared (NIR) LiDAR for the river corridor during a period of low flow on 21 September 2008 (24.35 m^3/s upstream of DPD and 17.61 m^3/s downstream of DPD). Boat-based SBS was acquired by Environmental Data Solutions during 2008 low flow conditions (~ 25.5–42.5 m^3/s) in August and September. A limited amount of SBS surveying was conducted at higher flows in March and May 2009 (~ 200–370 m^3/s). Key data gaps were surveyed using total station, RTK GPS, and SBS methods in November 2009. These areas largely consist of shallow backwater, side-channel, and near-bank areas that were unlikely to experience significant change during the higher flows of March and May 2009. Overall point densities are presented in Table S6.

Table S6. Density of data for the 2006/2008 topographic map

Geomorphic Reaches	3-TBR (2006)	All Else (2008)
Bathymetric Resolution	0.28 pts/m2	0.60 pts/m2
Terrestrial Resolution	0.11 pts/m2	5.54 ts/m2

S4.1.2. QA/QC

To ensure that the data sets were accurate and comparable, overlapping data sets were compared between ground-based and boat-based surveys and ground-based and LiDAR surveys. In addition, the accuracy of ground-based surveys was checked at known benchmarks. Overall, the mean differences among the survey methods were within the river's mean grain size (97mm).

For SBS data compared to the total station surveys, 50% of the data is within 0.15 m, 75% of the data is within 0.18 m, and 94% of the data is within 0.3 m. 8769 ground-based RTK GPS points were compared to the LiDAR data along flat surfaces. 54% of LIDAR points were within 0.03 m, 84.7% of LIDAR points were within 0.061 m, and 98.7% were within 0.12 m. Regular total station control point checks yielded accuracies of 0.0091-0.018 m. RTK GPS observations had vertical precisions of 0.018 m. Comparison of LiDAR water edge points versus the RTK GPS yielded observed differences of 30% within 0.03 m, 57% within 0.061 m and 92% within 0.15 m.

S4.2. 2014 Topographic Map Supplements

S4.2.1. Data Collection

Data for the 2014 LYR topographic map comprises of airborne bathymetric LiDAR, multi-beam sonar (MBS), single-beam sonar (SBS), and real-time kinematic (RTK) GPS survey points. The vast majority of the data comes from the airborne bathymetric LiDAR, which uses a green laser to penetrate the water column and a near-infrared (NIR) laser that provides better delineation of terrestrial features. MBS data was used to fill in the data gaps in deep pools where the green LiDAR was not able to penetrate through to the streambed, and SBS and RTK-GPS survey points were used to fill in the few remaining gaps and places where aquatic vegetation affected the LiDAR returns. Table S7 outlines each survey method, location(s), and date(s) of acquisition.

Table S7. Data sources for 2014 Lower Yuba River

Data	Location(s)	Dates(s)
SBS	1-EDR	2013
SBS	2-NR Pool	5/29/13-5/30/13,
SBS	2-NR	10/16/13-10/18/13
RTK-GPS	2-NR	9/11/13, 11/25/13
RTK-GPS	Backwater in 6-DPDR	3/6/13-2/6/14
MBS	LYR pools except in 2-NR & 1-EDR	8/11/14-8/14/14
NIR & Green LiDAR	All LYR	9/27/14
RTK-GPS	backwater in 6-DPDR	4/2/15
SBS	data gaps below DPD	6/3/15
RTK-GPS	data gaps below DPD	6/3/15
SBS	Dry Creek confluence	6/8/15
RTK-GPS	Dry Creek confluence	6/8/15, 6/16/15

Updated Coordinated System

All of the data, except for the 2014 LiDAR, was collected in California State Plane Zone 2 NAD83 U.S. Survey Feet. In 2011 there was an update to the NAD83 datum and the 2014 LiDAR data was collected using the 2011 update, California State Plane Zone 2 NAD83 (2011) U.S. Survey Feet. All other survey data has been re-projected into this new coordinate system in ArcGIS, including the 2006/2008 mapping efforts, to allow direct comparisons.

Airborne Bathymetric LiDAR Data

Quantum Spatial, Inc. (Sheboygan, WI) collected combined near-infrared (NIR) and green LiDAR data on 27 September 2014 during a period of low flow, approximately

15.3 m^3/s above Daguerre Point Dam (DPD) and 11.3 m^3/s below DPD. Low flows expose more of the river corridor for the NIR laser and reduce the depth needed for the green laser to penetrate through the water column. Processing of the data by Quantum Spatial, Inc. (QS) prior to delivery included:

1) Resolving the kinematic corrections for aircraft position data and developing a smoothed best estimate of trajectory (SBET).
2) Calculating the laser point positions using the SBET.
3) Performing a manual relative accuracy calibration using the tie-plane methodology and filtering erroneous points.
4) Using ground classified points to test relative accuracy (i.e. agreement between overlapping flight lines). Performing line-to-line calibrations for attitude parameters (pitch, roll, heading), mirror flex, and GPS drift.
5) Creating a water's edge breakline to distinguish between bathymetric returns and terrestrial returns.
6) Correcting for refraction through the water column for bathymetric returns.
7) Classifying the resulting data into ground (includes bathymetric points), water surface, water column, noise, and default (includes structures, vegetation, and noise) point classes.
8) Assessing the statistical absolute accuracy via direct comparisons of ground classified points to ground control survey data.
9) Manually reviewing and finalizing data classifications.
10) Generating 3.0 foot resolution bare earth and highest return rasters.
11) Exporting 1.5 foot NIR and green laser intensity rasters.

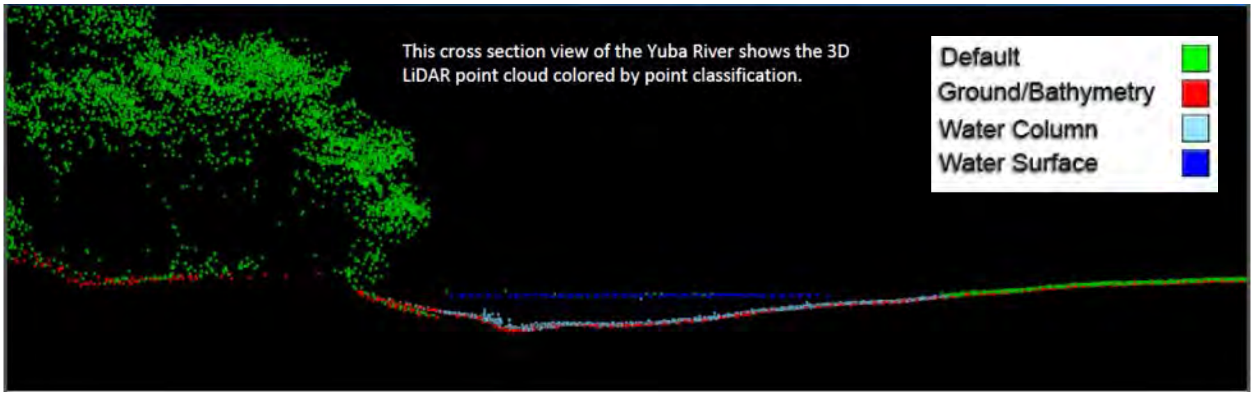

Fig. S3. Cross-section showing Quantum Spatial's LiDAR point classifications.

Fig. S3 shows a cross-section of the LiDAR data with the point classifications that QS used. The water surface points come from reflectance off the water surface by the NIR laser. The ground/bathymetry points come from the green and NIR laser in the terrestrial environment and only the green laser within the wetted channel. Note how there appears to be many ground returns that exist within the default classification in bare earth areas.

Good water clarity allowed the green laser to penetrate approximately 3-3.5 meters in depth (Fig. S4) yielding over 90% coverage of the streambed for LYR. First return densities give a representation of the number of laser pulse returns per area (excluding echoes). The data shows that actual point densities far exceeded the target point densities with first return point densities for the green and NIR sensors above 12 pts/m^2 (Table S8).

Table S8. First return point densities

First Return Type	Target Point Density	Actual Point Density
Green Sensor	4 pts/m^2	13.50 pts/m^2
NIR Sensor	8 pts/m^2	12.23 pts/m^2
Combined	12 pts/m^2	25.67 pts/m^2

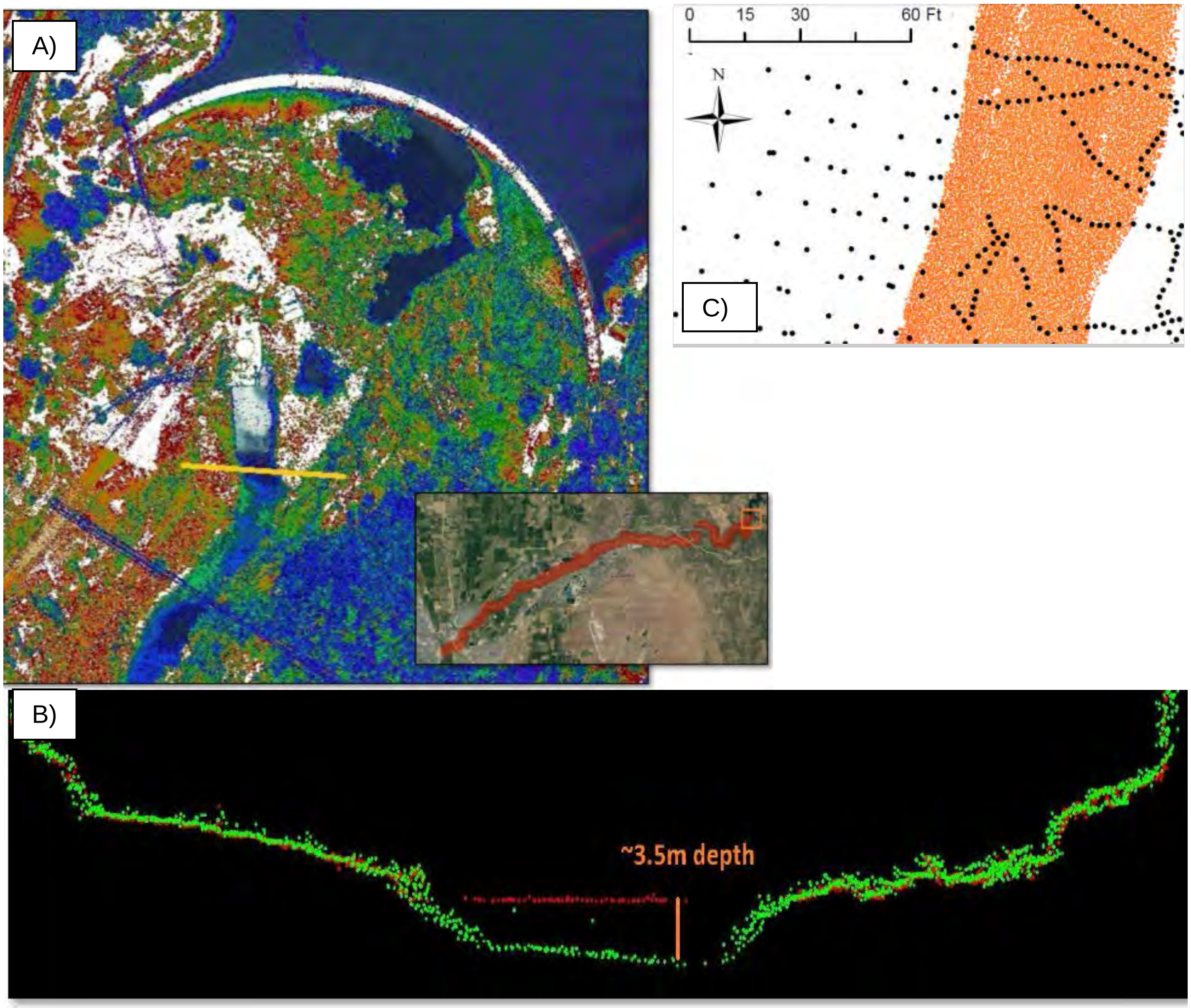

Fig. S4. A) Plan view of LiDAR returns colored by intensity below Englebright Dam. B) Profile view of the Englebright Dam pool which shows the penetration depth of the green LiDAR (shown in green) and reflectance off the water surface by the NIR LiDAR (shown in red). C) Contrasting the previous total station and single-beam sonar mapping (black dots) in 3-TBR with the density of the current multi-beam sonar data (orange dots).

After ground points were classified by QS, the density of ground points was analyzed and is presented in Table S9.

Table S9. Ground classified point densities

Ground Return Type	Point Density
All Ground Classified Returns	3.96 pts/m^2
Bathymetric Bottom Returns	2.30 pts/m^2

Absolute accuracy is an estimate of the error of the LiDAR derived ground surface when compared to a more accurate survey method. QS compared the LiDAR ground surface to 23 ground check points and 24 bathymetric check points that were developed from an RTK-GPS survey. The Fundamental Vertical Accuracy (FVA) is a measure of error reported at the 95% confidence level, i.e. 1.96*Root Mean Square Error (RMSE). The FVA for ground points and bathymetric points is 0.123 ft and 0.384 ft, respectively (Table S10).

Table S10. Summary of absolute accuracy statistics

	Sample	Average	Median	RMSE	Standard Deviation	FVA
Ground Check Points	23	0.008 m	0.006 m	0.019 m	0.018 m	0.038 m
Bathymetric Check Points	24	0.030 m	0.042 m	0.060 m	0.052 m	0.117 m

Relative accuracy is an estimate of the internal consistency of the LiDAR data. It is checked by comparing the identification of the same surface by overlapping flight lines. QS calculated the relative accuracy of the NIR and green laser using 125 and 122 surfaces, respectively. The relative accuracy reported at the 95-percentile, 1.96*Standard Deviation (SD), is 0.032 m and 0.048 m for the NIR and green lasers, respectively (Table S11).

Table S11. Summary of relative accuracy statistics

	Sample	Average	Median	RMSE	Standard Deviation	1.96*SD
NIR Laser (terrestrial)	125 surfaces	0.030 m	0.043 m	0.047 m	0.016 m	0.032 m
Green Laser (bathymetric)	122 surfaces	0.049 m	0.076 m	0.072 m	0.025 m	0.048 m

Multi-beam and Single-beam Sonar Data

The MBS data was collected over a period of four days from 11-14 August 2014 when flows on LYR were 40.0 m^3/s above DPD and 22.7-24.5 m^3/s below DPD. The higher water levels facilitate overlapping of the MBS and LiDAR data. The MBS data covers most of the deep pools from the confluence of the Yuba with the Feather River to the Narrow's canyon where a rapid prevents upstream access by boat. The MBS data has an average point density of 43.7 pts/m^2. Fig. S4c shows a visual comparison of the density of MBS points compared to previous SBS and total station mapping in 3-TBR.

SBS data was collected in 1-EDR upstream of 2-NR to Englebright Dam in 2013 by kayak. SBS data was also collected by jet boat on 3 June 2015 to fill in the remaining small data gaps in areas below DPD and on 8 June 2015 by kayak where Dry Creek flows into the lower Yuba River.

The MBS and SBS data were filtered and compared to the LiDAR data to determine their offsets and relative accuracy.

RTK-GPS Data

Several small areas that were affected by vegetation were surveyed with an RTK-GPS, including a backwater area in 6-DPDR called the Blue Lagoon, the Dry Creek tributary, and a few small backwater areas below DPD.

S4.2.2. Correcting Missing Boulder and Bedrock Data

Although QS classified the LiDAR data using automated algorithms, careful inspection revealed that significant areas of boulders and exposed bedrock features were filtered out of the ground/bathymetry point classification (Fig. S5). In general, bare-earth areas were smoothed out (i.e., over-filtered) and topographically complex features like boulders and exposed bedrock were often removed entirely as if the points were vegetation. LiDAR intensity imagery clearly distinguished these areas as bare earth, warranting additional filtering, but a trade-off exists between retaining fine-scale topography and erroneously classifying non-ground returns (e.g., low-lying vegetation or small man-made structures) as ground. Thus, a two-stage filtering process was developed to return the over-filtered points to the ground and bathymetry classification without introducing erroneous data.

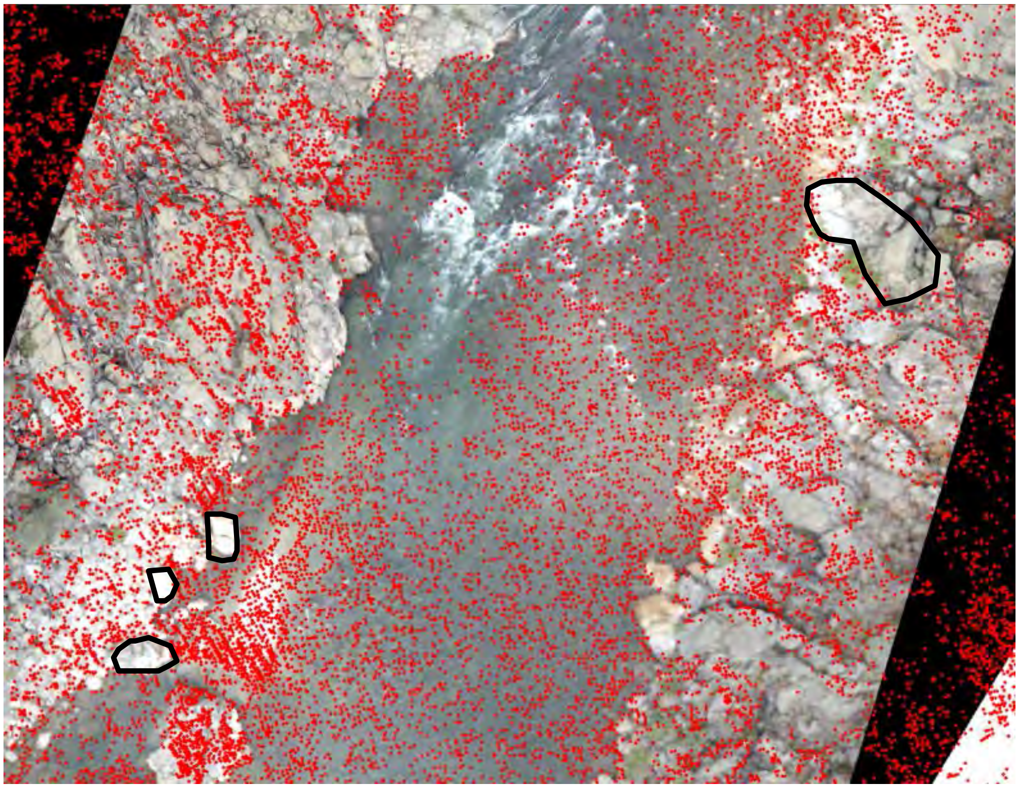

Fig. S5. Several examples of over-filtered ground returns outlined in black in the Englebright Dam reach, but the phenomenon is widespread throughout the image. Low cracks in the bedrock received many points as evident by lines of points and higher bedrock tops were filtered out leaving them unrepresented in the ground/bathymetry point file.

Improving Identification of Terrestrial Rock Features

The first step was to take all of the returns not classified as ground, and identify a new ground surface using the lasground_new.exe program within LAStools (Gilching, Germany), which uses a variation of Axelsson (2000) to generate an adaptive triangulated irregular network (TIN). The user must select a “step size”, which controls the size of the grid cells that initialize the TIN by choosing the lowest point in each grid cell. Smaller step sizes allow for finer-scale features to be identified in the ground-detection process. The “-wilderness” setting was used for filtering this data, which uses a three-meter step size. A second stage of filtering removed the areas that are influenced by vegetation or structures by creating a clip polygon of vegetated areas and man-made features. This was done by using additional tools within LAStools that distinguish between vegetation and structures by calculating the standard deviation of points above the ground-identified surface. Fig. S6 shows an example of the data after the LiDAR points have been reclassified and Fig. S7 shows the resulting land cover raster. Finally, a polygon file is made that includes the areas where points should not be added back into the ground point classification: vegetated ground, water, and structures. This polygon was visually verified and adjusted, where necessary, by using the LiDAR intensity imagery, the 2014 NAIP normalized-difference vegetation index, and the first-return elevation raster. This process ensures that only points from the bare-earth land cover are added back to the ground classification.

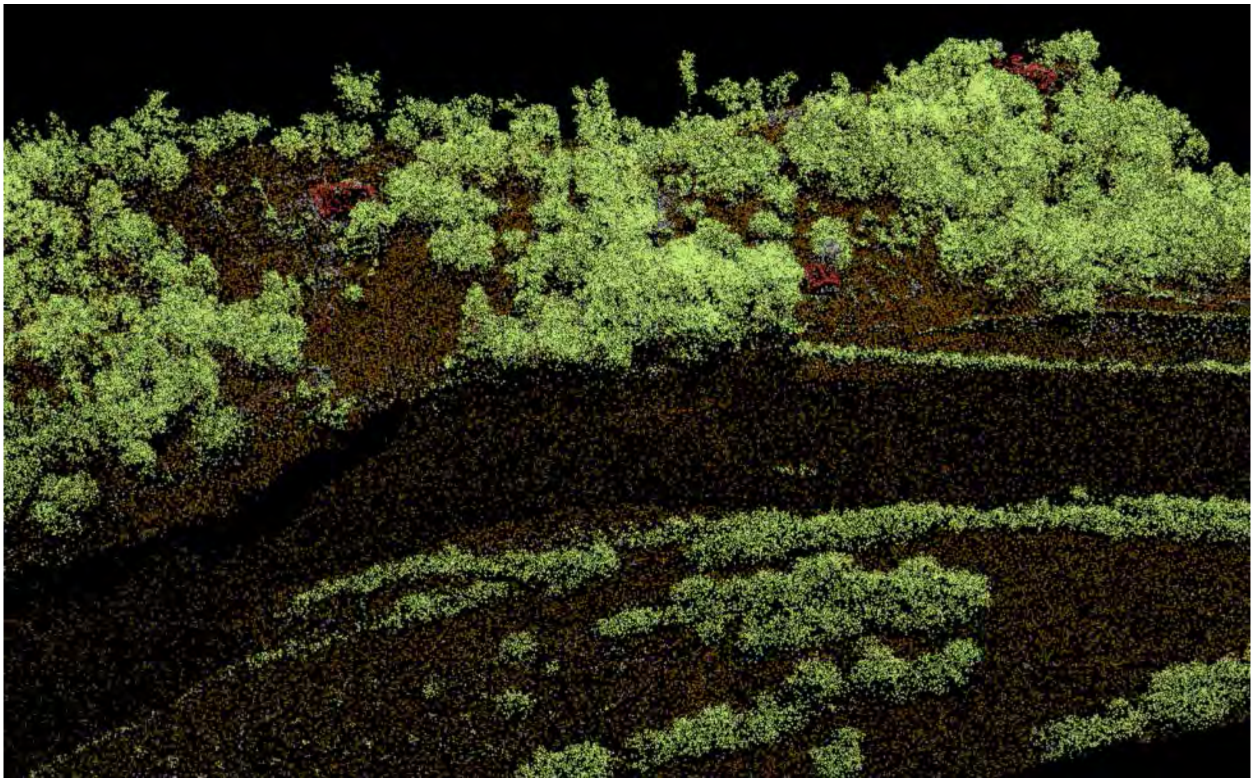

Fig. S6. Lidar points after reclassifying the default points. Vegetation is green, ground is brown, and structures are red.

Fig. S7. Land cover raster showing vegetation as green, water as blue, and bare-earth as light brown.

Delineating In-Channel Rock Features

Many of the in-channel areas where there were exposed or submerged rocks suffer from low surrounding point densities making ground classification unreliable (e.g., a large boulder in an otherwise deep pool that is void of bed returns). In these areas, rock features were manually delineated by visualizing the LiDAR point clouds in ArcGIS and confirming their presence with aerial imagery.

Results from Re-filtering

The points added back into the ground/bathymetry classification improved the resolution of the land surface without introducing significant errors. After this process was completed, the resulting point densities for bare earth areas increased from approximately 4pts/m^2 to 13pts/m^2 and the added detail within the map is visually apparent Fig. S8.

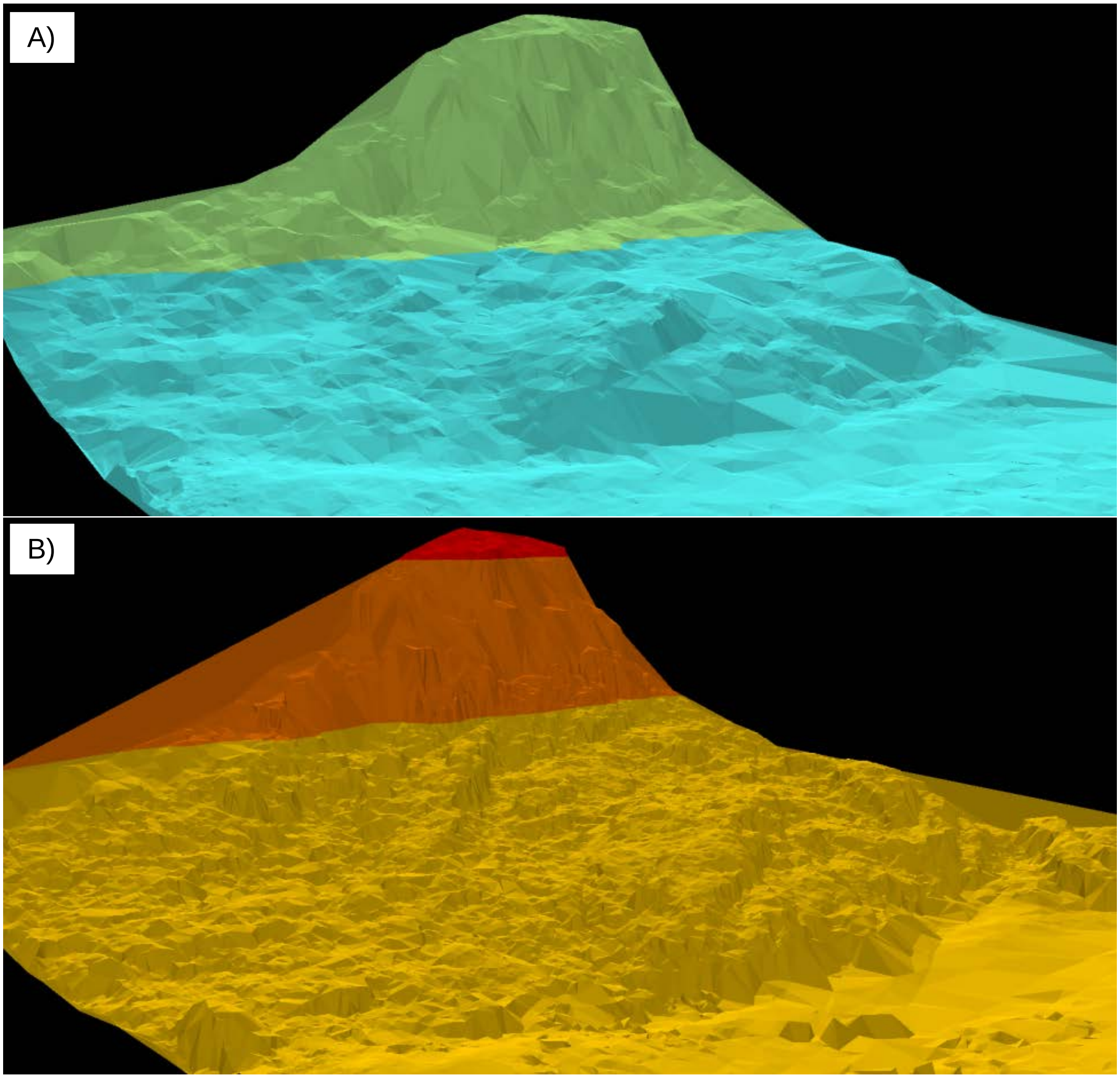

Fig. S8. A) An oblique view of a section of the Englebright Dam Reach before refiltering the data. B) That same view after the data was refiltered. Notice the presence of new boulder/bedrock clusters.

S4.2.3. Merging Data

The LiDAR data serves as the reference datum for all other survey point inputs. In order to merge the MBS and SBS data with the LiDAR data, the sonar data had to be filtered to remove bad returns caused by things like suspended sediment, bubbles, or vegetation. Then the sonar points were compared to the nearest LiDAR points and analyzed for systematic offset as detailed below.

Filtering Multi-beam and Single-beam Sonar Data

The SBS data is too sparse to use filtering algorithms like LAStools, so the best way to assess the quality of the data is to compare it to the LiDAR (if nearby LiDAR points exist) and/or visualize the data in 3D. Using a TIN colored by slope values, spires and elevated plateaus of points that are caused by bubbles or sediment are easily located and removed.

The MBS data can be filtered just like the LiDAR data using lasground_new.exe in LAStools, but issues with horizontal offsets may exist when comparing the sonar data to the LiDAR data. These areas can be quickly identified by spatially joining the MBS data to the nearest LiDAR point and highlighting the points with the largest vertical offsets. There are two probable causes of these horizontal offsets. First, the cliff face could be overhung such that the MBS is correctly identifying undercut caverns beneath the overlying terrain whose surface the LiDAR is mapping. This might occur for bedrock walls and cohesive hillsides. For jumbles of boulders and riprap, it is similarly possible that the MBS is obtaining returns through connected pore spaces deep into the pile. Second, it is very likely that there are “multipath errors”. These occur when some or all MB signals do not take a direct path back to the detector, and instead reflect off one or more other surfaces. This adds extra travel time causing an apparent extra distance. This is likely when there are vertical boundaries close to horizontal ones, such as when the boat is close to a steep bank or bridge pier. In at least some of the cases, we know that the MBS data is misbehaving because this issue occurs along vertical bridge piers where the LiDAR and MBS data should be in agreement. Thus, unless there is on-site evidence that the cliff face is overhung, the LiDAR data should be used to delineate the edges where the two data sources do not agree.

Merging the Multi-beam and Single-beam Sonar Data with the LiDAR Data

After the MBS and SBS data are filtered, the sonar points can be compared to the LiDAR points to assess vertical offsets. The goal for maximum precision and accuracy is to make a unique shift for each dataset rather than lump all of the data and do one shift. First, a polygon is created to clip the LiDAR points that overlap with the sonar data. Then, using the spatial join tool in ArcGIS, the LiDAR points that are within 5 cm horizontally of the sonar data are analyzed for their vertical offsets. To calculate the needed offset, the mean signed error for all the points that have a vertical difference of less than 0.3048 m (1 ft) was used. After applying the shifts, the vertical offsets were re-analyzed and the mean error assessed for all the points to verify that the shift performed as expected. Table S12 summarizes the number of observations, mean error, and standard deviations for the sonar and LiDAR comparisons.

Table S12. Vertical Comparisons of the Shifted Sonar Points to the LiDAR Points

	MBS and LiDAR Comparisons					SBS and LiDAR Comparisons		
Reach	8-MR/7-HR	6-DPDR	4-PBR	3-TBR	2-NR	6-DPDR	2-NR	1-EDR
Number of points	13127	9323	25156	71529	11925	5029	117	505
Mean Error [m]	0.008	0.003	-0.012	-0.001	0.058	-0.015	0.013	-0.002
St. Dev. [m]	0.11	0.08	0.16	0.08	0.07	0.11	0.20	0.18

S5. Analytical Methods Supplements

S5.1. DEM Uncertainty Supplements

The survey error, *SE*, represents the ability to accurately detect the ground surface. In this DEM uncertainty method, *SE* is estimated for three different land cover classes: bare earth, water, and vegetated ground.

For the bare earth land cover, LiDAR points from the 2008 and 2014 data sets were compared to each other on road surfaces throughout the study area. Points that were within 5 cm of each other in the horizontal direction were compared for their vertical differences. Assuming that the road surface hasn't changed over that time period, this analysis provides a representation of the relative accuracy of the LiDAR to repeatedly identify a bare ground surface. 1033 comparisons were made yielding a standard deviation of 0.039 m (Table S13).

Table S13. Comparisons between points less than 5 cm apart in the horizontal direction for the 2008 and 2014 LiDAR data sets on road surfaces throughout the lower Yuba River.

N	Mean Error [m]	Median [m]	Standard Deviation [m]
1033	0.000	0.001	0.039

For wetted areas, there are not surfaces that can be identified as static over the study period. However, the vertical agreement between the 2014 LiDAR and 2014 MBS data sets provide a good estimate of the relative accuracy of detecting the ground surface within the water. These comparisons are presented in Table S12 and yielded a standard deviation of 0.074m.

Lastly, for vegetated areas, a review of literature for vertical errors in LiDAR for forested settings was conducted (Table S14). Due to the LiDAR being flow during leaf-on conditions in August and September, the studies that represent those conditions (Reutebuch et al., 2003; Gould et al., 2013; Edson and Wing, 2015) present the best comparisons. Reviewing the list of relevant studies, 0.30 m was chosen for vegetated ground areas, which is within the range of reported RMSEs.

Table S14. Vertical errors in ground detection for LiDAR in forested settings.

Study	Vegetation Type	RMSE [m]	Slope Degrees	Leaf on/off
Reutebuch et al. (2003)	conifer forest	0.32	wide range	On
Hodgson and Bresnahan (2004)	Brush/low trees	0.233	4.2	Off
Hodgson and Bresnahan (2004)	Deciduous	0.259	2.5	Off
Gould et al. (2013)	Isolated *Ceanothus*	0.207	<14	On
Gould et al. (2013)	Continuous *Ceanothus*	0.433	<14	On
Tinkham et al. (2013)	Shrub	0.18	7.9	Off
Tinkham et al. (2013)	*Ceanothus*	0.30	8.9	Off
Tinkham et al. (2013)	Deciduous	0.20	6.5	Off
Edson and Wing (2015)	2:1, Conifer to deciduous	0.38	17	On
Edson and Wing (2015)	2.5:1, Conifer to Deciduous	0.37	17	On

In conclusion, *SE* for bare ground, water, and vegetated ground was 0.039 m, 0.074 m, and 0.30 m, respectively. These values compare well with the LiDAR absolute and relative accuracy statistics provided by QS for terrestrial and bathymetric points (Table S10 & Table S11). No parallel test is available for assessing the value chosen for the vegetated ground *SE*.

S5.2. Sediment Budget Supplements

Fig. S9 shows an example of the station boxes that were used to create longitudinal profiles of volumetric change and percent area of scour and fill.

Fig. S9. Station boxes used for creating longitudinal profiles of erosion and deposition volumes and percent area. The boxes are 1.524 m wide (5-ft), orthogonal to the valley centerline, and clipped to the width of the river valley.

S6. Results Supplements

See the attached overview maps of the 2006/2008 – 2014 topographic change results.

Supplementary References

Axelsson, P., 2000. Dem generation from laser scanner data using adaptive tin models. International Archives of Photogrammetry and Remote Sensing, 33(B4/1; PART 4), 111-118.

Brasington, J., Rumsby, B.T., Mcvey, R.A., 2000. Monitoring and modelling morphological change in a braided gravel-bed river using high resolution gps-based survey. Earth Surface Processes and Landforms, 25(9), 973-990.

Brierley, G.J., Fryirs, K., 2000. River styles, a geomorphic approach to catchment characterization: Implications for river rehabilitation in bega catchment, new south wales, australia. Environmental Management, 25(6), 661-679.

Carley, J.K., Pasternack, G.B., Wyrick, J.R., Barker, J.R., Bratovich, P.M., Massa, D.A., Reedy, G.D., Johnson, T.R., 2012. Significant decadal channel change 58–67years post-dam accounting for uncertainty in topographic change detection between contour maps and point cloud models. Geomorphology, 179, 71-88.

Edson, C., Wing, M.G., 2015. Lidar elevation and dem errors in forested settings. Modern Applied Science, 9(2), 139.

Gould, S.B., Glenn, N.F., Sankey, T.T., Mcnamara, J.P., Spaete, L.R., 2013. Influence of a dense, low-height shrub species on the accuracy of a lidar-derived dem. Photogrammetric Engineering and Remote Sensing, 79(5), 421-431.

Grant, G.E., Swanson, F.J., Wolman, M.G., 1990. Pattern and origin of stepped-bed morphology in high-gradient streams, western cascades, oregon. Geological Society of America Bulletin, 102(3), 340-352.

Hawkins, C.P., Kershner, J.L., Bisson, P.A., Bryant, M.D., Decker, L.M., Gregory, S.V., Mccullough, D.A., Overton, C.K., Reeves, G.H., Steedman, R.J., Young, M.K., 1993. A hierarchical approach to classifying stream habitat features. Fisheries, 18(6), 3-12.

Heritage, G.L., Milan, D.J., Large, A.R.G., Fuller, I.C., 2009. Influence of survey strategy and interpolation model on dem quality. Geomorphology, 112(3-4), 334-344.

Hodgson, M.E., Bresnahan, P., 2004. Accuracy of airborne lidar-derived elevation: Empirical assessment and error budget. Photogrammetric Engineering and Remote Sensing, 70(3), 331-339.

Kraus, K., Karel, W., Briese, C., Mandlburger, G., 2006. Local accuracy measures for digital terrain models. Photogrammetric Record, 21(116), 342-354.

Lane, S.N., Westaway, R.M., Murray Hicks, D., 2003. Estimation of erosion and deposition volumes in a large, gravel-bed, braided river using synoptic remote sensing. Earth Surface Processes and Landforms, 28(3), 249-271.

Lindsay, J.B., Ashmore, P.E., 2002. The effects of survey frequency on estimates of scour and fill in a braided river model. Earth Surface Processes and Landforms, 27(1), 27-43.

Mandlburger, G., Hauer, C., Wieser, M., Pfeifer, N., 2015. Topo-bathymetric lidar for monitoring river morphodynamics and instream habitats-a case study at the pielach river. Remote Sensing, 7(5), 6160-6195.

Milan, D.J., Heritage, G.L., Large, A.R.G., Fuller, I.C., 2011. Filtering spatial error from dems: Implications for morphological change estimation. Geomorphology, 125(1), 160-171.

Newson, M., Newson, C., 2000. Geomorphology, ecology and river channel habitat: Mesoscale approaches to basin-scale challenges. Progress in Physical Geography, 24(2), 195-217.

Passalacqua, P., Belmont, P., Staley, D.M., Simley, J.D., Arrowsmith, J.R., Bode, C.A., Crosby, C., Delong, S.B., Glenn, N.F., Kelly, S.A., Lague, D., Sangireddy, H., Schaffrath, K., Tarboton, D.G., Wasklewicz, T., Wheaton, J.M., 2015. Analyzing high resolution topography for advancing the understanding of mass and energy transfer through landscapes: A review. Earth-Science Reviews, 148, 174-193.

Pasternack, G., Tu, D., Wyrick, J., 2014. Chinook adult spawning physical habitat of the lower yuba river, Prepared for the Yuba Accord River Management Team. University of California, Davis, Davis, CA.

Reutebuch, S.E., Mcgaughey, R.J., Andersen, H.E., Carson, W.W., 2003. Accuracy of a high-resolution lidar terrain model under a conifer forest canopy. Canadian Journal of Remote Sensing, 29(5), 527-535.

Sawyer, A.M., Pasternack, G.B., Moir, H.J., Fulton, A.A., 2010. Riffle-pool maintenance and flow convergence routing observed on a large gravel-bed river. Geomorphology, 114(3), 143-160.

Tinkham, W.T., Hoffman, C.M., Falkowski, M.J., Smith, A.M.S., Marshall, H.P., Link, T.E., 2013. A methodology to characterize vertical accuracies in lidar-derived products at landscape scales. Photogrammetric Engineering and Remote Sensing, 79(8), 709-716.

Wadeson, R., 1994. A geomorphological approach to the identification and classification of instream flow environments. Southern African Journal of Aquatic Science, 20(1-2), 38-61.

Wechsler, S.P., Kroll, C.N., 2006. Quantifying dem uncertainty and its effect on topographic parameters. Photogrammetric Engineering and Remote Sensing, 72(9), 1081-1090.

Wheaton, J.M., Brasington, J., Darby, S.E., Kasprak, A., Sear, D., Vericat, D., 2013. Morphodynamic signatures of braiding mechanisms as expressed through change in sediment storage in a gravel-bed river. J. Geophys. Res.-Earth Surf., 118(2), 759-779.

Wheaton, J.M., Brasington, J., Darby, S.E., Merz, J., Pasternack, G.B., Sear, D., Vericat, D., 2010a. Linking geomorphic changes to salmonid habitat at a scale relevant to fish. River Research and Applications, 26(4), 469-486.

Wheaton, J.M., Brasington, J., Darby, S.E., Sear, D.A., 2010b. Accounting for uncertainty in dems from repeat topographic surveys: Improved sediment budgets. Earth Surface Processes and Landforms, 35(2), 136-156.

Wheaton, J.M., Darby, S.E., Sear, D.A., 2008. The scope of uncertainties in river restoration, River restoration: Managing the uncertainty in restoring physical habitat, pp. 21-39.

Wheaton, J.M., Fryirs, K.A., Brierley, G., Bangen, S.G., Bouwes, N., O'brien, G., 2015. Geomorphic mapping and taxonomy of fluvial landforms. Geomorphology, 248, 273-295.

Wyrick, J., Pasternack, G., 2012. Landforms of the lower yuba river, University of California, Davis, CA.

Wyrick, J.R., Pasternack, G.B., 2015. Revealing the natural complexity of topographic change processes through repeat surveys and decision-tree classification. Earth Surface Processes and Landforms.

Wyrick, J.R., Senter, A.E., Pasternack, G.B., 2014. Revealing the natural complexity of fluvial morphology through 2d hydrodynamic delineation of river landforms. Geomorphology, 210, 14-22.